Lysosomal signalling pathways influence heart rhythm, and regulate atrial function

Rebecca A. Capel[1#], Emily Akerman[1#], Eva A. Rog-Zielinska[2], Annika Winbo[3], Daniel Aston[4], Razik Bin Abdul Mu-u-min[1], Matthew J. Read[1], Samuel J. Bose[1], Pawel Swietach[5], Jingyu Wang[6], Alexander D. Corbett[7], Andreas Koschinski[5], Florian Falter[4], Serena Calamaio[8], Dario Melgari[8], Rachele Prevostini[8], Ilaria Rivolta[8], Thamali Ayagama[5], Ifan Jenkin[1], Jillian N. Simon[9], Funsho E. Fakuade[11abc], Julius R. Pronto[11abc], Parveen Sharma[12], Qianqian Song[1], Martin J Booth[6], Frances M. Platt[1], Ming Lei[1], Svenja Hester[13], Roman Fischer[10], Niels Voigt[11abc], Ulrich Schotten[13], Sander Verheule[13], Antony Galione[1], Marco Keller[14], Franz Bracher[14], Manuela Zaccolo[5], Derek A. Terrar[o1], Rebecca A. B. Burton[o*1,15]

[1]Department of Pharmacology, University of Oxford, Oxford, UK.

[2] Institute for Experimental Cardiovascular Medicine, University Heart Center and Faculty of Medicine, University of Freiburg, Freiburg, Germany.

[3] Department of Physiology, Manaaki Manawa, University of Auckland, New Zealand.

[4]Department of Anaesthesia and Critical Care, Royal Papworth Hospital NHS Foundation Trust, Papworth Road, Cambridge Biomedical Campus, Cambridge, CB2 0AY.

[5]Department of Physiology, Anatomy and Genetics, University of Oxford, Oxford, UK.

[6]Department of Engineering Science, University of Oxford, Oxford, UK.

[7]Department of Physics and Astronomy, University of Exeter, Exeter, UK.

[8]Cellular Electrophysiology Unit, Institute of Molecular and Translational Cardiology, IRCCS, Policlinico San Donato, 20097 San Donato Milanese, Italy.

[9]Aging + Cardiovascular Discovery Center, Lewis Katz School of Medicine at Temple University, Philadelphia, PA.

[10]Target Discovery Unit, University of Oxford, Oxford, UK.

[11a]Institute of Pharmacology and Toxicology, University Medical Center Göttingen, Göttingen, Germany.

[11b]DZHK (German Center for Cardiovascular Research), Partner Site Göttingen, Germany.

[11c]Cluster of Excellence "Multiscale Bioimaging: from Molecular Machines to Networks of Excitable Cells" (MBExC), University of Göttingen, Göttingen, Germany.

[12]Cardiovascular and Metabolic Medicine, Institute of Life Course and Medical Sciences, University of Liverpool, Liverpool, UK.

[13]Departments of Physiology and Cardiology, Cardiovascular Research Institute Maastricht, Maastricht University, Maastricht, The Netherlands.

[14]Department of Pharmacy, Center for Drug Research, Ludwig-Maximilians University, Munich, Germany.

[15]Department of Pharmacology and Therapeutics, Institute of Systems, Molecular and Integrative Biology, University of Liverpool, Liverpool, UK.

[#]Joint first authors

[o]Joint senior authors

*Corresponding author: rebecca.burton@pharm.ox.ac.uk, r.a.b.burton@liverpool.ac.uk

Abstract

In the heart, endogenous nicotinic acid adenine dinucleotide phosphate (NAADP) triggers lysosomal calcium (Ca^{2+}) release to augment sarcoplasmic reticulum [1] Ca^{2+} sequestration, producing larger Ca^{2+} transients. However, the role of lysosomal Ca^{2+} signals in pacemaker activity, a distinct Ca^{2+}-operated function of the sinoatrial node (SAN), or in the atrial myocardium has not been investigated. Pharmacological or genetic ablation of the NAADP pathway inhibits the spontaneous beating rate response to β-adrenergic stimulation in intact SAN. We found intracellular signalling microdomains between lysosomes and neighboring SR or mitochondria in mouse, rabbit, goat, and human atrial tissue. The spatial relationship between lysosomes and other Ca^{2+}-handling organelles are altered in goat and human atrial fibrillation. Furthermore, we demonstrate atrial myocytes produce 3′–5′-cyclic adenosine monophosphate in response to lysosomal signalling, adding a novel trigger for cyclic nucleotide signalling. Our findings support the hypothesis that lysosomal Ca^{2+} signalling directly increases cardiomyocyte cAMP and modulates pacemaker activity.

Introduction

Nicotinic acid adenine dinucleotide phosphate (NAADP) is one of the most potent second messengers in the calcium (Ca^{2+}) signalling cascade [2], triggering the release of Ca^{2+} from acidic stores, such as lysosomes, via two-pore channels (TPC) [3, 4]. NAADP-mediated acidic Ca^{2+} store signalling has been found to affect cellular physiology and pathology in numerous cell types and species, highlighting lysosomes as significant contributors to various signalling mechanisms [5].

In the heart, NAADP is synthesized in response to beta(β)-adrenergic stimulation [6-8]. Inhibition of the NAADP pathway significantly inhibits physiological responses to acute β-adrenergic stimulation [6, 8-10] and is protective against arrhythmias caused by high-dose acute or chronic isoprenaline exposure [10]. However, observations regarding the importance of NAADP in atrial signalling have, thus far, focused solely on the effects of a single dose of isoprenaline in isolated myocytes, and studies in intact tissue are lacking.

The heart's intrinsic pacemaker, the sinoatrial node (SAN), is highly sensitive to Ca^{2+}, being driven by a coupled system of Ca^{2+} and membrane clocks [11]. As well as the SR-driven Ca^{2+} clock [12, 13], there are a large number of additional Ca^{2+}-modulated processes within pacemaker myocytes [14, 15]. These include Ca^{2+} stimulation of adenylyl cyclases (ACs) [16, 17], and Ca^{2+}/calmodulin-dependent protein kinase II (CaMKII) [18]. Recently, proteomic studies implicated the role of lysosomes in physiological atrial function and their potential contribution to the development of atrial fibrillation (AF) [19]. Further, immunohistological studies of the autophagosome marker microtubule-associated protein 1 light chain 3 (LC3) and lysosome marker lysosome-associated membrane protein 1 (LAMP1) have shown that the contents of both autophagosomes and lysosomes are much greater in SAN cells than in atrial or ventricular cardiomyocytes [20]. Contribution of lysosomal Ca^{2+} signalling to the control of SAN pacemaker activity has not previously been studied.

The autonomic nervous system, and particularly adrenergic/cholinergic balance, has a profound influence on the risk of AF [21]. In sustained or persistent AF, fibrillating atria undergo both structural and functional remodelling, including significant changes in cellular Ca^{2+} handling and β-adrenergic responses [21]. Changes in lysosome quantity and function have been demonstrated in patients with several cardiac conditions [22], including those with atrial septal defects, in whom AF is a common complication [19]. Furthermore, degenerative changes, such as the accumulation of lysosomes, have been found to correlate with atrial cellular electrophysiological changes in disease [23].

In healthy cardiac ventricular myocytes, lysosomes form membrane contact sites (MCSs) with both the SR and mitochondria, the presence of which could indicate that lysosomes form functional Ca^{2+} signalling microdomains with both organelles [24]. It is possible that lysosomal changes in atrial disease are associated with changes in the number or functionality of MCSs. Lysosome position and structure of MCSs in healthy cardiac atrial myocytes and in AF are currently unknown. Here, we provide

evidence consistent with a role for lysosomal Ca^{2+} signalling as part of the β-adrenergic response in both atrial and, for the first time, the SAN, tissue and cells, including the novel aspect of NAADP-mediated modulation of cellular 3′-5′-cyclic adenosine monophosphate (cAMP) pools.

Additionally, we provide evidence that lysosomal location and MCSs with the SR and mitochondria change as part of the cellular structural remodelling that occurs during AF.

Results

Lysosomal calcium contributes to the β-adrenergic response in the SAN pacemaker

Physiological or genetic ablation of the NAADP signalling pathway inhibits the spontaneous beating rate response to β-adrenergic stimulation in intact SAN tissue.

Single cell data has provided evidence that NAADP-mediated stimulation of lysosomal Ca^{2+} signalling in either isolated atrial [25] or ventricular [6] myocytes causes an increase in Ca^{2+} transient amplitude and SR Ca^{2+} content. This pathway has been reported to contribute to the cellular β-adrenergic response, but previous work focused on isolated single cells, was limited to a single dose of isoprenaline, and did not consider any potential contribution to SAN pacemaking.

The right atrium contains the SAN and was therefore used to investigate responses of the murine SAN by monitoring changes in spontaneous beating rate during cumulative dose-response additions of isoprenaline (Fig. 1a).

Intact SAN preparations responded to cumulative additions of isoprenaline (0.1-1000nM) with an increase in rate presenting an expected sigmoidal pattern. In the presence of 0.001 % DMSO, a solvent control, cumulative doses of isoprenaline led to an increase in beating rate, the maximum rate response was 80% (79-82) with an EC_{50} of 2.2nM (1.9-2.5) (Fig. 1b). We used different pharmacological approaches to modulate lysosomal Ca^{2+} signalling. We used 500nM bafilomycin A1 to abrogate acidic Ca^{2+} store loading by inhibition of V-ATPase proton pump. The maximum beating rate increase during cumulative isoprenaline additions was comparable to control at 85% (83-89) increase from baseline, however there was a significant rightward shift in the EC_{50}, to 9.5nM (7.9-11.6) (Fig. 1b). The NAADP binding site antagonist *trans*-Ned-19, at 3µM, led to both a significant rightward shift in the EC_{50} for isoprenaline (3.7nM (3.2-4.4)) as well as a significant reduction in the maximum beating rate increase, to 63% (61-65) (Fig. 1a-b). No significant differences were observed in baseline beating rate before inhibitor additions and neither inhibitor affected spontaneous beating rate in the absence of stimulation with isoprenaline (Fig. 1c-d).

The potential contribution of the NAADP pathway to pacemaker physiology was also explored using genetic tools. Preparations containing the intact spontaneously-beating SAN from wild-type [26] C57BL/6NCrl mice recorded a maximum acceleration of 76% (69-83) with an EC_{50} of 2.7nM (1.9-3.9) in response to isoprenaline. TPC2 is the lysosomal Ca^{2+} release channel opened upon NAADP binding [3, 4]. SAN preparations from $TPC2^{-/-}$ mice exhibited a blunted acceleration in response to isoprenaline (maximum 52% (42-62)) with no significant difference in EC_{50} (Fig. 1e).

CD38, which belongs to the ADP-ribosyl cyclase family, catalyzes synthesis of both NAADP and cyclic ADP-ribose [27]. Atrial preparations from $CD38^{-/-}$ mice exhibited a significantly reduced response to

10nM isoprenaline which was not further reduced in the presence of bafilomycin A1 whilst in dye-loaded, spontaneously beating intact SAN preparations from WT mice, addition of 10nM isoprenaline led to a significant increase in spontaneous beating rate generated by the SAN. This increase was significantly reduced in the presence of bafilomycin A1 [28].

Intact left atrial studies were also conducted to investigate the change in contractile force (inotropy) in response to isoprenaline (data presented in Supplementary Fig. 1). These observations provide further evidence that abrogation of lysosomal Ca^{2+} signalling reduces atrial contraction in response to β-adrenergic stimulation.

Physiological ablation of the NAADP signalling pathway inhibits the spontaneous beating rate response to β-adrenergic stimulation in isolated, spontaneously beating guinea pig sino-atrial node myocytes.

We confirmed these observations at the single cell level in isolated, spontaneously beating guinea pig SAN myocytes, using Fluo-5F-AM to monitor the generation of spontaneous Ca^{2+} transients. SAN myocytes were identified by morphology and the presence of rhythmic, spontaneous beating (Fig. 2a). Following superfusion with physiological salt solution (PSS), isolated SAN cells loaded with 3μM Fluo-5F-AM in PSS demonstrated spontaneous Ca^{2+} transients in both groups (Fig. 2b and c). In PSS, the control group had a spontaneous beating rate of 116±17bpm (n=4), superfusion with 0.001% DMSO (a solvent control) did not significantly alter this rate (128±20bpm, n=4, Fig. 2d). Before addition of a pharmacological agent, a second group of cells had a spontaneous beating rate of 145±13bpm which did not significantly differ to DMSO group (n=4, Fig. 2d). The addition of 100nM bafilomycin A1 did not significantly alter this beating rate (157±18bpm, n=4). Superfusion of 3nM isoprenaline accelerated spontaneous beating rate by 76.5±6.6% (n=4) in DMSO condition (Fig. 2e). Following the addition of 3nM isoprenaline, cells exposed to 100nM bafilomycin A1 accelerated by 43±5% (n=4) (Fig. 2e), a response significantly lower than the control group. Maximum response was observed after 2 minutes of 3nM isoprenaline exposure in both conditions (Fig. 2f). There was no significant difference in Ca^{2+} transient amplitude between bafilomycin A1 and DMSO-treated groups, when applied either alone (Fig. 2g), or after exposure to 3nM isoprenaline (Fig. 2h and 2i).

Physiological ablation of the NAADP signalling pathway inhibits the spontaneous beating rate response to β-adrenergic stimulation in spontaneously beating cardiomyocytes derived from human-induced pluripotent stem cells.

We used spontaneously beating cardiomyocytes derived from human-induced pluripotent stem cells (hiPSC-CM, Winbo differentiation protocol) to investigate the effect of bafilomycin A1 in a spontaneously beating human cell model. As seen in SAN myocytes (Fig. 2), hiPSC-CM loaded with Fluo-5F-AM (Fig. 3a) demonstrated spontaneous Ca^{2+} transients (Fig. 3b-c). Spontaneous beating rate following the addition of DMSO or 100nM of bafilomycin A1 did not differ (Fig. 3d); baseline beating

rates were 47±2bpm (n=14, N=4) and 50±3bpm (n=11, N=3) in the presence of DMSO and in 100nM of bafilomycin A1 respectively (Fig. 3d). Additionally, no significant difference in Ca^{2+} transient amplitude was observed between DMSO and bafilomycin A1 prior to stimulation with isoprenaline (Fig. 3e). Superfusion of 3nM isoprenaline in control conditions significantly increased spontaneously beating rate over the course of 4 minutes in control conditions, with a maximum increase of 35.4±7.1% at 4 minutes (Fig. 3f). In contrast, bafilomycin A1-exposed hiPSC-CM showed a maximum increase of 8.7±5.3% after 1 minute of exposure, with no further increase (Fig. 3f). The Ca^{2+} transient amplitude of the hiPSC-CM decreased over 3nM isoprenaline exposure in both conditions but to a significantly greater extent in the presence of 100nM bafilomycin A1 (Fig. 3c and 3g).

Lysosomal signalling contributes significantly to the increase in cellular cAMP levels in response to β-adrenergic stimulation

Although the concentration of Ca^{2+} reported to reside within an acidic store is high, 400-600μM in macrophages [29], the proportion of acidic stores contributing to a given signal and the time course of this contribution is unknown. Immunostaining of lysosomes using LAMP2 antibody was conducted on fixed NRAMs to confirm the presence of lysosomes in neonatal cultured atrial cardiomyocytes used for all FRET experiments (Fig. 4a). We performed super resolution imaging on NRAM cells labelled with LAMP2 to identify individual lysosomes (Fig. 4b). This was done based on spot quality (a function of both absolute value and local contrast). 342 lysosomes were identified within an individual cell (Fig. 4b). Of these, 296 (87%) were found to be located within 500nm of their nearest neighbour (yellow spheres, Fig. 4b and Supplementary Fig. 2a). A size distribution of the lysosomes was also acquired **(**Supplementary Fig. 2b). Owing to the stochastic nature of single molecule switching (in which fluorophores spend the majority of time in a dark state) and the fact that large regions of the cell were obscured by drift correction beads, the absolute value of the lysosome volume measured from the SMS data should be considered an underestimate of the true volume. Based on these limitations and using an estimate of the neonatal cell volume of $1000\mu m^3$ [30] a lower limit on the volume fraction of the lysosomes can be estimated as $0.3\mu m^3/1000\mu m^3$ (0.3%). Estimates from the literature report lysosomes make up just 0.08±0.4% of cell volume in rat heart [31].

Lysosomal Ca^{2+} release in response to NAADP leads to an increase in SR Ca^{2+} content and Ca^{2+} transient amplitude without affecting sarcolemmal Ca^{2+} flux [6, 10]. Given the shift in EC_{50} observed in the aforementioned tissue studies (Fig. 1b), one possible explanation which has been observed in other cell types [32] but not previously considered in cardiac myocytes is lysosomal signalling which may result in altered cellular cAMP. We measured cellular cAMP in cultured neonatal rat atrial myocytes (NRAMs) expressing the cytosolic fluorescence resonance energy transfer (FRET)- based reporter EPAC-S^{H187} (Fig. 4c) [33].

In the presence of 0.1% DMSO (a solvent control) 1nM isoprenaline led to a FRET change of 30.05±3.6% (n=11, N=5). This increase in cellular cAMP in response to β-adrenergic stimulation was significantly reduced if undertaken in the presence of 100nM bafilomycin A1 (8.5±2.3%, n=4, N=4, P<0.01, Fig. 4d). Addition of 1nM isoprenaline to NRAMs in a zero- Ca^{2+} solution resulted in a FRET change of 11.39±0.9% (n=4, N=4), with a significant reduction when isoprenaline was added in the presence of 100nM bafilomycin A1 (4.34±0.6%, n=4, N=4, P<0.001, Fig. 4e). These observations suggest that lysosomal Ca^{2+} contributes significantly to the cellular cAMP increase which forms a central component of β-adrenergic responses, and that this contribution is independent of sarcolemmal Ca^{2+} flux.

A lysosomal contribution to cellular cAMP could feasibly occur downstream to changes in SR and cytosolic Ca^{2+} levels and/or in the vicinity of the lysosome itself. After 45 minutes of incubation with ryanodine and thapsigargin (RyThap, both at 2μM) to empty SR stores, and in the absence of extracellular Ca^{2+}, administration of 1nM isoprenaline resulted in a 17.47±1.2% (n=6, N=5) FRET change. The presence of 100nM bafilomycin A1 continued to significantly inhibit (3.7±1%, n=7, N=5, P<0.0001, Fig. 4f) the cellular cAMP response to isoprenaline. We confirmed the presence of lysosomes in our NRAMs by staining with LAMP2 antibodies and confocal imaging (Fig. 4a) as well as super resolution (Fig. 4b). Taken together these observations suggest that lysosomal signalling, activated following β- adrenergic stimulation, is able to modulate cellular cAMP levels by a mechanism which does not require Ca^{2+} arising from the SR.

FRET experiments were carried out on atrial cardiomyocytes derived from human-induced pluripotent stem cells (hiPSC-aCM) expressing the cytosolic FRET-based reporter EPAC-S^{H187} [33]. Live cell imaging with Lysotracker was conducted to confirm presence of lysosomes in hiPSC-aCM (Fig. 4g). Upon β-adrenergic stimulation with 1nM isoprenaline a FRET peak was observed of 42.51±4.6% (n=7, N=4) indicating an increase in cAMP levels. Peak of FRET change in response to 1nM isoprenaline in the presence of 100nM bafilomycin A1 was significantly lower (19.42±2.2%, n=8, N=4, P<0.01, Fig. 4h).

The presence of the atrial-specific ultrarapid delayed rectifier potassium current (I_{Kur}) served as the marker for assessing atrial differentiation in hiPS-aCM. Patch-clamp experiments were conducted on hiPS-aCM and hiPS-CM **(**Supplementary Fig. 3ai-ii**)**. I_{Kur}, characterized by its sensitivity to 4-aminopyridine (4-AP), was detected in all of the hiPS-aCM, across three independent rounds of differentiation, with an average density of 1.9±0.3 pA/pF (n=11) when measured at 50 mV **(**Supplementary Fig. 3b**)**. Immunofluorescence staining for specific atrial markers demonstrates their presence in cardiomyocytes differentiated using an atrial-like cell protocol, as depicted in the images, revealing the presence of $K_v1.5$ **(**Supplementary Fig. 3c**)**, responsible for the I_{Kur}, and the presence of pro-ANP accumulated in the perinuclear region and in cytoplasmic granules **(**Supplementary Fig. 3d**).**

Lysosomal signalling contributes significantly to the increase in cellular cAMP levels in response to TPC2 stimulation

Lysosomal signalling acts directly to increase cellular cAMP level via TPC2 channels on lysosomes [10]. In the presence of 0.001% DMSO, 10µM of the direct TPC2-activator TPC2-A1-N [34] led to a 26.28±2.7% (n=7, N=5) FRET change. After 45 minutes incubation with ryanodine and thapsigargin in a zero- Ca^{2+} solution, the response to 10µM TPC2-A1-N was not changed (20.91±2%, n=6, N=6, P>0.05, Fig. 5a). These observations show a significant increase in cellular cAMP in response to direct stimulation of lysosomal Ca^{2+} release. Incubations of 100nM bafilomycin A1 and 3µM *trans*-Ned- 19 significantly reduced the FRET change to 13.64±2.1% (n=6, N=4, P<0.05) and 10.83±1.4% (n=6, N=4, P<0.01) respectively, but did not abolish this response (Fig. 5a).

CaMKII activity has previously been reported to be upstream of cAMP accumulation and findings report CaMKII to stimulate cAMP production by activating ACs [40]. However, studies have not been conducted on cardiomyocytes and a downstream effector(s) for this accumulation, has not yet been identified. We observe significant decrease in FRET change in the presence of 1µM KN-93 (11.57±2.7%, n=4, N=4, P<0.05) in response to 10µM TPC2-A1-N compared to control (26.28±2.7%, n=7, N=5, Fig. 5b), linking Lysosomal Ca^{2+}release to CaMKII activity. To further investigate this, we ran FRET experiments in the presence of 3µM of the specific AC1 inhibitor ST034307 and observed a significantly smaller increase in cAMP levels in response to 10µM TPC2-A1-N (13.18±2.7%, n=4, N=4, P<0.05) compared to control (26.28±2.7%, n=7, N=5, Fig. 5b), raising the potential that the contribution of this mechanism could be augmented under physiological conditions. We have also conducted immunolocalisation studies of AC1 and LAMP2 on isolated SAN guinea-pig myocytes showing colocalization (Fig. 5c), illustrating that Ca^{2+} release via lysosomes may directly lead to activation of Ca^{2+}-sensitive AC1 in SAN myocytes.

Lysosomes form microdomains with the sarcoplasmic reticulum and mitochondria in cardiac atria and SAN

Previously, electron microscopy studies of rabbit cardiac ventricular myocytes have demonstrated lysosomes to be in close proximity to both the SR and mitochondria, thereby constituting a plausible signalling microdomain [24]. Thin-section 2D transmission electron microscopy (TEM) of tissue samples from rabbit atria identified lysosomes with a maximum diameter of 278±16.3nm (Fig. 6a). Lysosomes observed in atrial myocytes also consistently formed plausible MCSs with the SR and mitochondria (Fig. 6b). The shortest measured distance between a lysosome and its nearest SR was 17.2±1.3nm (n=12, Fig. 6a), conforming to the definition of an MCSs as being <30nm [35]. Mitochondria were also observed in close proximity to lysosomes in atrial myocytes with the shortest

measured distance between a lysosome and its nearest mitochondrial membrane in atrial myocytes of 24.8±6.6nm (Fig. 6a).

2D TEM may underestimate the size or overestimate the distance between two structures due to the lack of control over the plane and angle of the section not always including the shortest distance [24]. Measurements were therefore performed in 3D which allowed us to minimize the artifacts associated with 2D imaging. These measurements were made in electron tomogram of rabbit atria, and the lysosome maximum diameter was measured to be 663nm, shortest lysosome-SR distance was 6.4nm and shortest lysosome-mitochondria distance was 7.6nm (Fig. 6c-d).

Additional measurements were performed in rabbit and mouse SAN electron tomograms (Supplementary table. 1). In rabbit SAN maximum diameter of lysosomes was 299.5nm, the shortest lysosome-SR distance was 5.6nm (n=1) and shortest lysosome-mitochondria distance was 5.3nm (n=1). In murine SAN tissue lysosomes had a maximum diameter of 432±20.3nm (n=9), lysosomal membranes were observed to be in close apposition to both SR (10.42±2nm, n=9) and mitochondrial membranes (5.03±0.5nm, n=9). Example murine SAN images from electron tomograms can be seen in Fig. 6e-f and Supplemental Video 1.

Lysosomal size and position are altered during atrial disease

Lysosomal size and position in a large animal model of AF.

We measured the size and position of lysosomes in relation to both the SR and mitochondria in left atrial tissue in a goat AF model using 3D electron tomography. Lysosomes in control, sham-operated samples had a maximum diameter of 286.2±17.2nm (n=37 lysosomes in N=4 goats; Fig. 7a). Lysosomes were observed in close apposition to the SR (14.1±1.5nm at the closest point, n=35, Fig. 7b), with 92% of lysosome-SR pairs forming likely MCSs (being <30nm apart) indicating formation of a possible lysosome-SR microdomain. Lysosomes from goats in sinus rhythm, however, did not commonly form MCSs with mitochondria. The average lysosome was a minimum of 185.5±31.9nm (n=35) away from the nearest mitochondria (Fig. 7c) with only 23% forming MCSs.

After 6 months in AF, atrial lysosomes were significantly larger than those observed in sinus rhythm controls (maximum diameter 479.1±54.3nm, n=18 lysosomes from N=4 goats, $P<0.05$ vs control, Fig. 6a). Lysosomes in AF tissue were also positioned significantly further away from the SR, at a mean distance of 19.45±1.9nm (compared to 14.11±1.49nm in sham-operated samples) between the lysosome and nearest SR, with 88% of lysosome-SR pairs forming MCSs ($P<0.05$ vs control (92%), Fig. 7b). Lysosomes in AF goats were significantly closer to mitochondria than those in control cells, with the average closest distance of 74.9±17.6nm (n=16, Fig. 7d-e image of tomogram and model, Supplementary Fig. 4, Supplemental Video 2 and 3). This was combined with a shift to 44% of lysosomes forming MCSs in AF (from 23% in samples from sham-operated controls).

Discussion

We present evidence that lysosomal Ca^{2+}, acting through NAADP-mediated stimulation of TPC2 channels, contributes significantly to the physiological modulation of heart rate at the SAN pacemaker and highlight a previously unknown contribution to cardiac cellular signalling in which lysosomal Ca^{2+} directly modulates cAMP upstream to the previously reported effects on SR Ca^{2+} content and Ca^{2+} handling.

In spontaneously beating right atrial preparations, abolition of lysosomal Ca^{2+} signalling at multiple stages of the NAADP signalling pathway, either pharmacologically (bafilomycin A1, *trans*-Ned-19) or genetically ($TPC2^{-/-}$) led to a reduction in maximal response ($TPC2^{-/-}$), rightward shift in EC_{50} (bafilomycin A1), or both (*trans*-Ned-19) in response to Isoprenaline. Despite being potentially predictable given the Ca^{2+} dependence of SAN pacemaking and ubiquitous nature of the lysosomal system, these are to our knowledge the first published observations demonstrating lysosomal Ca^{2+} signalling contributing to physiological control of SAN pacemaker rate. These observations correlated with our experiments on isolated SAN myocytes, where bafilomycin A1 significantly reduced cellular acceleration seen during subsequent β-adrenergic stimulation (Fig. 2). Bafilomycin A1 alone did not have a significant effect on cellular beating rate or Ca^{2+} transient amplitude. In contrast to observations published in atrial [25] and ventricular myocytes [6], this may suggest that lysosomal Ca^{2+} signalling is not constitutively active in the SAN. We also conducted single cell experiments monitoring intracellular pH over time and to ensure that bafilomycin A1 had no effect on cytoplasmic pH (Supplementary Fig. 5).

One intriguing explanation for the rightward shift in EC_{50} for isoprenaline seen in tissue preparations after inhibition of lysosomal Ca^{2+} signalling, is the possibility that lysosomal Ca^{2+} signalling may affect cellular cAMP. We performed FRET in cultured NRAM to monitor cytosolic cAMP and found that inhibition of lysosomal Ca^{2+} signalling, or the NAADP pathway, reduced cellular cAMP accumulation during response to a single dose of isoprenaline (Fig. 4). This inhibition was maintained not only when experiments were undertaken in the absence of extracellular Ca^{2+}, but also in those undertaken following depletion of the SR by pre-incubation with 2μM ryanodine and thapsigargin. These observations are consistent with the contribution of lysosomal Ca^{2+} signalling during β- adrenergic stimulation including the modulation of cAMP in the vicinity of lysosomes themselves and not requiring the NAADP-stimulated increase in SR Ca^{2+} content [25] as an upstream requirement.

TPC2-A1-N has recently been shown to activate endogenous TPC2 channels [39]. Direct stimulation of TPC2 channel opening using TPC2-A1-N [34] caused a significant increase in cellular cAMP which was significantly reduced if the agonist was applied after incubation with either bafilomycin A1 or *trans*-Ned-19. Previous studies on NAADP signalling in cardiomyocytes have demonstrated that the increased Ca^{2+} transient amplitude observed following the addition of NAADP was abolished in the

presence of CaMKII inhibitors KN-93 or AIP [10]. CaMKII activity has been reported to be upstream of cAMP accumulation, findings report CaMKII to stimulate cAMP production by activating ACs [40]. A downstream effector for this accumulation, however, has not yet been identified. We observe significant decrease in FRET change in the presence of 1µM KN-93 (11.57±2.7%) in response to TPC2-A1-N compared to control (26.28±2.7%, Fig. 5b). It is not implausible that, via a similar mechanism in cardiomyocytes, Ca^{2+} release from the lysosome could lead to CaMKII activation via Ca^{2+}/CaM and enhance cAMP production through another as of yet unknown interaction leading either to stimulation of an AC or inhibition of a phosphodiesterase. In other cell types, Ca^{2+} release from lysosomes via purinergic P2RX4 channels has been shown to stimulate cAMP production via Ca^{2+} stimulated AC1 [41]. AC1 is CaM-dependently stimulated [41]. AC1 is CaM-dependently stimulated [42] with an EC_{50} for Ca^{2+} of 75nM [43]. Ca^{2+} release from lysosomes into localised signalling microdomains could feasibly drive cAMP formation by Ca^{2+}/CaM-mediated AC1 stimulation. AC1 activation has previously been shown to lead to downstream CaMKII activation through protein phosphatase 1 as an intermediary [44, 45]. This is one plausible mechanism by which localized Ca^{2+} release leading to cAMP accumulation may activate CaMKII and explain our previously published observations in which functional CaMKII was a pre-requisite for NAADP-mediated increase in Ca^{2+} transient amplitude [10].

Perturbation of lysosomal Ca^{2+} signalling led to around a 50% reduction in cellular cAMP accumulation in response to isoprenaline, whether in normal extracellular solution, zero Ca^{2+} solution, or after depletion of SR calcium. Of note, FRET experiments were carried out on quiescent myocytes whereas Ca^{2+} transient and contractile force experiments took place on electrically stimulated myocytes. Gul and co-workers, also using quiescent myocytes, reported that NAADP pathway inhibition completely abolished the cardiac ventricular myocyte response to isoprenaline [8]. It would seem unlikely, however, that the sole gatekeeper to β-adrenergic signalling in the heart is the lysosome. Indeed, β-adrenergic stimulation leads to a range of cellular effects known to be independent of the lysosomal pathway. For instance, exogenous NAADP has no effect on L-type Ca^{2+} current [6, 25], and neither does NAADP pathway inhibition alter the increase in I_{CaL} stimulated by isoprenaline [10]. Our observations, and those of Gul et al, support the hypothesis that in the absence of continuous Ca^{2+} cycling, the proportion of the isoprenaline response attributable to lysosomal Ca^{2+} signalling is relatively high. In the presence of Ca^{2+} transients, however, this is likely to be more balanced. That said, stimulation of AC1 activity by Ca^{2+}/CaM, being one mechanistic suggestion, as AC1 has been reported to be significantly augmented in the presence of Gs activation such as that of isoprenaline signalling [46]. To investigate this, we ran FRET experiments in the presence of 3µM of the AC1 inhibitor ST034307 and observed a significantly smaller increase in cAMP levels in response to TPC2-A1-N (13.18±2.7%) compared to control (26.28±2.7%) and immunolocalisation studies of AC1 and LAMP2 on isolated SAN guinea-pig myocytes showed colocalization (Fig. 5b-c), raising the potential that the contribution of this mechanism could be augmented under physiological conditions.

It is interesting that acute inhibition of lysosomal Ca^{2+} signalling led to a change in EC_{50} or EC_{50} and maximum response, whereas constitutive knock-out of TPC2 led to a change in maximum response without affecting EC_{50}. We have not performed *in vivo* ECG recordings on WT and $TPC2^{-/-}$ mice in this study, but the spontaneous beating rates of WT and $TPC2^{-/-}$ right atrial preparations were not observed to be significantly different (Fig. 2c-d). It is possible that some compensatory changes could occur at either the autonomic or subcellular level. Regardless, perturbation of lysosomal Ca^{2+} signalling by either pharmacological or genetic means significantly affected β-adrenergic response in a manner consistent with a reduction in acceleration in response to isoprenaline during physiological signalling. Experiments on isolated SAN myocytes (Fig. 2), confirm the utility of this mechanism in physiological SAN cell modulation. Our observations in NRAMs, which have a phenotype appropriate to both atrial and SAN, specifically in terms of a synchronously-beating network [47], support a mechanism for this modulation which alters cellular cAMP accumulation in response to isoprenaline and would therefore be consistent with a lateral shift in the EC_{50} of isoprenaline during dose-response curve studies.

In cardiac ventricular myocytes, 3D tomography has previously revealed that lysosomes consistently form MCSs with both the SR and mitochondria [24]. Similar observations were made here in atrial and SAN cardiomyocytes across several species (Fig. 6-7). In contrast to observations in the ventricle, atrial lysosomes were found to form MCSs with mitochondria less often, with only 23% of lysosomes-mitochondria pairs forming MCSs (Fig. 7).

AF causes significant structural remodeling at both the cellular and tissue level [48]. We found that lysosomes were situated significantly further away from the SR and closer to mitochondria in goat AF tissue when compared to sham-operated controls (Fig.7). The change in mean distance between lysosomes and the SR was relatively modest, changing from 14.0±1.49nm in sham-operated to 19.5±1.89nm in AF samples, however this does not preclude its functional significance in the context of microdomain signalling. Fameli and co-workers previously investigated how spatial proximity may affect lysosome-ER microdomain signalling and found that gradually increasing lysosome-SR junctional width resulted in a concomitant decrease in lysosome-SR junctional Ca^{2+} concentration [49]. A further analysis of surface area contact between lysosome and SR will help in assessing the impact of these communications. We recently undertook a molecular characterization of lysosomes in the same goat model of AF used in this study and observed a downregulation of Ras-related protein 7a (Rab7). Rab7 normally present on late endosomes, is either directly or indirectly involved in each event occurring between early endosomes and lysosomes. RAB7A is a recruiting protein for the tethering molecules by regulating transport pathways and transforming late-endosomes to lysosomes (lysosomal biogenesis) and sorting complex required for transport pathways, after 6 months in AF [36]. Ly-SR distance increase in human AF is still to be fully quantified, future studies will seek to investigate whether this change could underpin the increase in lysosome-SR distance reported in our study and the potential functional impact of this change on the lysosomal Ca^{2+} signalling.

Migration of lysosomes closer to mitochondria or mitochondria movement towards lysosomes in AF is also of potential functional importance. Cytosolic Ca^{2+} is finely regulated via homeostatic mechanisms (principally by buffering within the SR, mitochondria and lysosomes) [49]. Davidson et al have showed that reperfusion-induced Ca^{2+} oscillations in primary adult cardiomyocytes can be suppressed by treatment with TPC inhibitor Ned-19, or, more effectively, with an improved form of *trans*-Ned-19 called Ned-K and genetic deletion of TPC1 was similarly protective in mice, highlighting that inhibition of NAADP on reperfusion following ischemia affords protection against reperfusion injury via the action on TPC1 [49]. In the context of the fibrotic phenotype of AF [50, 51], an increase from 23% of lysosomes forming MCS with mitochondria in sinus rhythm controls to 44% in AF could feasibly contribute to altered signalling between lysosomes and mitochondria, mitophagy and fibrosis.

Dysregulation in lysosomal calcium can subsequently affect the lysosome mediated Ca^{2+} signalling cascade and may be potentially arrhythmogenic. Studies show changes in lysosomal function/autophagy precede electrical remodelling [36]. We ran unbiased proteomics to access global protein changes in human right AF samples. As a caveat that we may not detect low abundant end-lysosomal proteins, we opted to perform data-independent acquisition parallel accumulation-serial fragmentation (DIA-PASEF) on human right atrial appendage tissue samples with label free protein quantification, a method for measuring low abundance proteins as it improves depth and quantitation of detected proteins (Supplementary Fig. 6a and b). Our proteomics analysis highlighted several lysosome and autophagy related proteins that were regulated including GAA in AF patients (Supplementary Fig. 6c). We also note metabolic changes in AF and activation of pro- apoptotic signalling pathways as noted by others [52]. Integrin signalling, methylmalonyl pathway, microautophagy signalling were the top canonical pathways identified in IPA (Supplementary Fig. 7a-d). Top Canonical Pathways include: Integrin Signalling (p-value 2.38E-06), Methylmalonyl Pathway (p-value 1.14E-05), Microautophagy Signalling Pathway (p-value 1.98E-05), Response to elevated platelet cytosolic Ca^{2+} (p-value 2.04E-05) and 2-oxobutanoate Degradation I (p-value 2.81E-05). Molecular and Cellular Function include Cellular Assembly and Organisation (p-value range 4.06E-03 – 5.97E-15), Cellular Function and Maintenance (p-value range 4.06E-03 – 5.97E-15), Cell Morphology (p-value range 4.06E-03 – 1.11E-08), Cellular Movement (p-value range 4.06E-03 – 1.47E-08) and Cellular Development (p-value range 3.00E-03 – 1.99E-08) (Supplementary Fig. 8a-j). Regulated proteins used in IPA are listed in Supplementary File 2 and Supplementary File 3 contains ingenuity canonical pathways analysis which includes molecules. Additionally, we observe changes in cardiac contractility proteins (Supplementary Fig. 9a-c). RyR2, Triadin and Calsequestrin 2 are significantly down regulated in AF. Expression levels of RyR2 have been found unaltered [54, 55] or reduced in dogs, goats, and cAF patients [56-58]. RyR2 sensitivity to cytosolic and luminal Ca^{2+} and thus its open probability are modulated by accessory binding proteins (e.g. calsequestrin, junctin,

triadin, FK506-binding protein 12.6 kDa [FKBP12.6]) and posttranslational modifications (e.g. phosphorylation) [59]. Changes in the relative amounts of junctin and triadin have been shown to alter RyR2 Ca^{2+} release and cause cardiac arrhythmias [60, 61]. The increased lysosomes-SR distance noted in AF tissue and change in size of lysosomes, dysregulation of signaling microdomains and alternation in the SR channels, open new questions to be answered relating to whether endolysosomes contribute to abnormal SR Ca^{2+} handling and therefore a role in AF maintenance.

As a first pass, we had access to biopsies from one AF and one sinus rhythm control (SinusR) patient (left atrial tissue) sample. We performed 2D transmission EM tile scans imaging and measured lysosome size and positioning using in 13 myocytes from the chronic AF patient and 10 myocytes from the patient in SinusR. We acknowledge this data is only from biopsies from 1 disease and control patient, therefore exert caution relating to conclusions (Supplementary Fig. 10a-c). In the myocytes of the chronic AF patient, lysosomes show an increase in diameter and occupy a higher cell volume compared to lysosomes in SinusR myocytes. Lysosomes were consistently observed to form MCSs with the SR in both human tissue samples. The distance between lysosomes and the SR significantly increases in chronic AF myocytes, consistent with our results obtained using goat samples ($P<0.0001$, Fig. 7c). Lysosomes were measured in transverse and longitudinal cross-sections of the myocytes. Outlines (in yellow dashes) of the measured cytosol area of the myocytes and lysosome-SR distances measured are presented representative images in Supplementary Fig. 10d-g. In a separate SinusR control left atrial patient sample, we performed EM tomography. Representative tomogram showing lysosomes in close proximity to SR and mitochondria in Supplementary Fig. 11 and Supplemental Video 4. These early EM data looking at lysosome-SR distances provides data that suggests microdomain signalling could be affected between the lysosomes and the SR, which could have important consequences on Ca^{2+} handling.

Very recently a study has highlighted that TPCs are important for cardiac contraction [62], relevant and related to our findings. We report a role for lysosomal Ca^{2+} signalling in pacemaking, as functionally important in β-adrenergic responses (Fig. 8a). A novel pathway in cardiomyocyte signalling, in which lysosomal Ca^{2+} release contributes directly to cellular cAMP is proposed and is in keeping with previously published observations regarding the importance of CaMKII (Fig. 8b). Autophagy has been shown to regulate Ca^{2+} mobilization in T lymphocytes through endoplasmic reticulum homeostasis [63] whether this is the case in atrial cardiac myocytes cells is yet to be discovered. Functional studies to ascertain lysosomal Ca^{2+} signalling in AF and integration with the molecular changes observed in lysosomes will be of significant pharmacological therapeutic value.

Acknowledgements

This study was supported by the Wellcome Trust and Royal Society (PI RABB: 109371/Z/15/Z). RABB is funded by the Wellcome Trust and British Heart Foundation (109371/Z/15/Z and (PG/18/4/33521). RABB acknowledges research funds from the Ellis T Davies Fellowship Endowment, University of Liverpool. SJB is a post-doctoral scientist funded by the British Heart Foundation (PG/18/4/33521). RABB holds a Senior Research Fellowship at Linacre College, Oxford. RAC is a post-doctoral scientist funded by the Wellcome Trust and Royal Society (109371/Z/15/Z). AW is supported by the Health Research Council of New Zealand (21/380). MZ is supported by the British Heart Foundation (RG/17/6/32944). TA received funding from the Returners Carers Fund (PI RABB), Medical Science Division, University of Oxford, the Nuffield Benefaction for Medicine and the Wellcome Institutional Strategic Support Fund (ISSF), University of Oxford. EA received funding from the Returners Carers Fund (PI RAC), University of Oxford. RABB acknowledges support from the Covid-19 Rebuilding Research Momentum Fund (CRRMF) Oxford Funds and Returning Carers Funding (Oxford). The Electron microscopy and Tomography work was also supported by German Research Foundation Collaborative Research Centre SFB1425 (DFG #422681845). We thank the SCI-MED imaging facility at the Institute for Experimental Cardiovascular Medicine in Freiburg for support in image analysis. ERZ is a German Research Foundation Emmy Noether Fellow (DFG #396913060). We acknowledge technical support from Dr Errin Johnson, Charlotte Melia and Raman Dhaliwal from the Dunn School of Pathology for Electron microscopy assistance. MK and FB received funding from German Research Foundation (project BR 1034/7-1). This research was funded in whole, or in part, by the Wellcome Trust [109371/Z/15/Z]. For the purpose of Open Access, the author has applied a CC BY public copyright license to any Author Accepted Manuscript version arising from this submission. We thank Prof Barbara Casadei, Oxford for access to tissue and Prof Peter Kohl, do access to laboratory equipment for use by ERZ. We thank Prof Galione's staff, Oxford for technical advice and help with animal breeding. We thank Prof Patrizia Dell'Era, Brescia Italy (sadly now deceased) for technical support and hiPSC-CM collaborations.

Authorship contribution statement

RABB and DAT: Conceptualisation, investigation, writing, reviewing and editing. RABB: Fund acquisition via the Wellcome Trust Fellowship. RC and EA: Lead experimentalists, formal analysis, writing, reviewing and editing – original draft. EAR-Z, NV, FEF, JRP: Electron microscopy, 3D tomography, human tissue work. AW, MR, SB, SC, DM, RP, IR: hiPSC Ca^{2+} transient and FRET experiments. DA, RBAM, FF: Animal electron microscopy analysis and CD38 experiments. PS: Baf-A1 pH experiments. TA, IJ, JNS, ML: Molecular biology experiments and pharmacology experiments. PS, SH, RF, RABB, TA: Human proteomics. QS, JW, MB, AC: Super resolution image preparation, imaging and analysis. FP, AG, MZ: Supervision, data discussion and interpretation. MZ, AK: FRET

supervision. US, SV: Goat AF model, physiology experiments and tissue collection. MK, FB: Drug chemistry and production of compounds.

Declaration of Competing Interest

None.

Data and code availability

Mass Spectrometry data has been deposited in PRIDE [Project accession: PXD042391]. Data can be requested by contacting the lead contact. This study did not generate new unique codes.

Inclusion & Ethics

This study follows inclusion and ethics in global research.

Online Methods

Animals

All animal experiments were performed in accordance with the United Kingdom Home Office Guide on the Operation of Animal (Scientific Procedures) Act of 1986. All experimental protocols (Schedule 1) were approved by the University of Oxford. Male New Zealand White rabbits, Sprague Dawley rat litters, guinea pigs, C57BL/6NCrl mice and CD-1 mice were obtained from Envigo or Charles River. The TPC2$^{-/-}$ mice were created as described previously [3, 4].

Contraction setup

As seen in methods previously published in [64]. Hearts from male CD1 mice were rapidly dissected and place in warm, oxygenated physiological saline solution (PSS, in mM: NaCl 125, $NaHCO_3$ 25, KCl 5.4, NaH_2PO_4 1.2, $MgCl_2$ 1, glucose 5.5, $CaCl_2$ 1.8, pH to 7.4 with NaOH and oxygenated with 95 % O2/5% CO2) containing heparin (10U/ml). In a dissection chamber, left (data presented in Supplementary Fig. 1) and right atria were cleared, separated, and mounted to a force transducer in an organ bath as ventricular tissue was discarded. The organ bath was filled with 37^{o}C oxygenated with 95% O2/5% CO2 PSS with a resting tension between 0.2-0.3g to visualise contraction. Tension data were digitised using a PowerLabs bridge amplifier and recorded on LabChart5 software (all from ADInstruments, UK). Chronotropic and Inotropic effects were measured in real-time using the Chart5 Ratemeter function. After left and right preparations had stabilised the effects of isoprenaline were investigated over a cumulatively increasing concentration range of 0.1nM to 1000nM, doses were administered every 3 minutes into the organ bath. Inhibitors were added 45 minutes before first addition of isoprenaline to ensure effects. Preparations were excluded if stabilised beating rate under control conditions in the presence of PSS only was under 300bpm or if preparations were arrhythmic.

Adult guinea SAN cell isolation

The methods were previously published by (Capel, 2015). Guinea pig hearts were dissected and washed in heparin-containing PSS (20 IU per mL) to prevent blood clots forming and mounted on a Langendorff

setup for retrograde perfusion via the aorta. The heart was fist perfused in a modified Tyrode solution containing (in mM): NaCl 136, KCl 5.4, $NaHCO_3$ 12, sodium pyruvate 1, NaH_2PO_4 1, $MgCl_2$ 1, EGTA 0.04, glucose 5; gassed with 95% O_2/5% CO_2 to maintain a pH of 7.4 at 37°C for 3 minutes. Solution was switched to a digestion solution: the modified Tyrode above containing 100µM $CaCl_2$ and 0.04mg/ml Liberase™ (Roche, Penzberg, Germany) and no EGTA. After 25 minutes of enzymatic digestion, the heart was removed. The right atrium was pinned in a dissection bath, opened by anterior incision, and the SAN was identified from anatomical features and tissue appearance. The SAN was dissected into thin strips (~2x5mm) followed by gentle trituration and stored in a high potassium medium (KB, in mM: KCl 70, $MgCl_2$ 5, K^+ glutamine 5, taurine 20, EGTA 0.04, succinic acid 5, KH_2PO_4 20, HEPES 5, glucose 10; pH to 7.2 with KOH) at 4°C.

Calcium transient imaging of guinea pig SAN cells

Isolated atrial myocytes were incubated with 3µM Fluo-5F-AM in SAN KB for 10 min at 37ºC in the dark. Cells were then plated onto a glass coverslip for 10 minutes to adhere before imaging. All recordings were at 37°C under gravity-fed superfusion. Cells were visualized using a Zeiss Axiovert 200 with attached Nipkow spinning disk confocal unit (CSU-10, Yokogawa Electric Corporation, Japan). Excitation light, transmitted through the CSU-10, was provided by a 488-nm diode laser (Vortran Laser Technology Inc., Sacramento, CA). Emitted light was passed through the CSU-10 and collected by an iXON897 EM-CCD camera (Oxford Instruments, UK) at 60 frames per second with 2×2 binning (pixel size = 0.66667µm^2). To avoid dye bleaching, video recordings were 10-20 seconds long with a frequency of 80 up to 100 frames per seconds. Ca^{2+} transients were measured using regions of interests (ROIs) in Andor iQ software (v 1.7) to record average whole cell fluorescence.

Neonatal cell isolation

NRAMs were isolated using a modified protocol from [65] and [66]. Hearts were dissected from 3-day-old Sprague Dawley rat pups, culled by cervical dislocation followed by exsanguination. Atria were separated from the ventricles and cut into 4 pieces. Atrial myocytes were digested enzymatically in trypsin (1mg/ml, Merck, UK) rocked at 4°C for 2 hours. Atrial myocytes were then enzymatically isolated a second time with collagenase (type IV, 1mg/ml, Merck, UK). Trypsin was replaced by 4ml collagenase solution and tissue was gently triturated using a plastic pipette for 1 min and then stirred gently in a water bath at 37°C for 2 minutes and the first supernatant was discarded. A further 4ml collagenase solution was added to the tissue pellet and triturated for 1 min using a wide bore pipette. This solution was then stirred gently in a bath at 37°C for 2 minutes and the supernatant (4ml) added to 3ml cold Hank's buffered salt solution (HBSS) and stored in a 15ml centrifuge tube on ice. This process was repeated a further 3 times to produce a total of 4x7ml cell suspensions. Tubes were centrifuged at 2000 revolutions per minute for 8 minutes. Supernatant was then removed, and the cells were resuspended in 2ml cardiomyocyte plating media (CPM: 67% DMEM, 17% M199, 10% horse serum, 5% FBS, 1% Penicillin/Streptomycin) before being centrifuged at 1000 revolutions per minute for 10

minutes. All samples were then strained using a sterile cell strainer (70µm). Isolated myocytes were pre-plated and incubated at 37°C (95% O2, 5% CO2) for 1 hour as a purification step to allow removal of fibroblasts. Myocytes were counted and seeded onto 24mm laminin (66µg/cm^2, Merck, UK) coated glass coverslips in 35mm 6-well plates at a density of 30,000 cells per well.

hiPSC-CM culture and cardiomyocyte differentiation (Winbo protocol)

The hiPSC-CMs were obtained from Dr Winbo [67], hiPSC-CM stem cell study approved by institutional review committees in Umeå, Sweden (Regional Ethics Committee, Umeå University: Dnr 05-127M), and Auckland, New Zealand (Health and Disability Ethics Committees: 17/NTA/226), and all the participants have provided written informed consent. As previously described, reprogrammed from peripheral blood mononuclear cells from a healthy adult male using an integration-free kit (CytoTune-iPS 2.0 Sendai Reprogramming Kit, Invitrogen, Life Technologies, now Thermo Fisher, Cat. Nos. A16517 and A16518) [67]. The hiPSC-CMs were differentiated into cardiomyocytes using previously published methods [67, 68]. Briefly, thawed hiPSC-CMs were plated on Geltrex™-covered 12-well plates (0.3x10^6 cells/well) and cultured in StemFlex™ medium. On day 0, at ~85% confluency, the culture medium was changed to RPMI/B27- insulin medium with 6µM GSK3-β inhibitor CHIR9902, followed by RPMI/B27-insulin medium with 5µM Wnt inhibitor IWR1 on day 3. From day 7, the cells were grown in RPMI/B27+insulin medium, replaced every 72 hours. Spontaneously beating cardiomyocytes were further matured to a minimum of 21 days post hiPSC-CM stage, then dissociated (Accutase™ (200µl/ well) for FRET or (Collagenase B 1mg/ml in RPMI/B27+insulin medium) Ca^{2+} transient imaging for 18 hours at 37°C for and replated on 12mm Geltrex™-covered glass coverslips before experiments.

hiPSC-CM cardiac culture (Calamaio protocol)

Both hiPSC-aCM lines used for all experiments were derived from healthy donors. In particular, one from a female donor with no diagnosed diseases (https://hpscreg.eu/cell-line/TMOi001-A, purchased from Thermo Fisher Scientific) [69] and the other, previously characterized and published from a 62-year-old male not affected by AF or other cardiac pathologies [70]. Approved protocols granted by the Ethical Committee of Brescia (protocol number 1737) and a written consent obtained from the patients, in agreement with the declaration of Helsinki. hiPSC-aCM lines were maintained on human Biolaminin 521 LN-coated dishes in TeSR-E8™ medium (Thermo Fisher Scientific).

Cardiac differentiation was carried out by monolayer culture on Matrigel® hESC-qualified Matrix (Corning, Corning, NY, USA) coated dishes using the PSC Cardiomyocytes Differentiation Kit (Thermo Fisher Scientific), following manufacturer instructions. To induce atrial differentiation, an adaptation of the method previously described [71] was used. Briefly, cells were treated with 1 µmol/L atRA (Sigma) starting from day 3 of differentiation, and the medium was changed every day until day 7. Then, cells were maintained in Cardiomyocytes Maintenance Medium (Thermo Fisher), changing

the medium every other day. On the 21st day of differentiation, hiPSC-aCM culture was enriched using the PSC-Derived Cardiomyocyte Isolation Kit (Miltenyi Biotech) following manufacturer instructions, which allows magnetic separation with highly specific CM surface markers. Immediately after magnetic separation, iPSC-CMs were collected and cryopreserved in liquid nitrogen. For the experiments, atrial differentiated hiPSC-aCM were thawed on Matrigel-coated dishes and maintained at 37°C (95% O_2, 5% CO_2) with Cardiomyocyte Maintenance Medium with B-27 Supplement 50X and penicillin/streptomycin 100X (Thermo Fisher Scientific). Cells were culture until 28 days before running FRET or live imaging.

Calcium transient imaging of hiPSC-CM

Spontaneously beating hiPSC-CM grown on 12mm coverslips were transferred to the Ca^{2+} imaging rig and incubated with 3µM Fluo-5F-AM in extracellular solution adjusted for use in hiPSC-CM-derived cardiomyocytes (in mM: NaCl 140, KCl 5.4, $CaCl_2$ 1.8, $MgCl_2$ 1, HEPES 10, D-Glucose 10) [72] for 15 minutes at 37ºC in the dark. Ca^{2+} transient imaging experiments were performed during continuous perfusion with 37ºC extracellular solution via an in-line heater. A control recording of spontaneous cardiomyocyte activity was obtained for 10 minutes before addition of DMSO (0.001%, Merck Life Science UK Limited) or bafilomycin A1 (100nM, Bio-Techne Ltd) for 10 minutes. Thereafter 3nM isoprenaline (Merck Life Science UK Limited) was added to the extracellular solution and Ca^{2+} transients recorded for 4 minutes. Recordings were done at 40 frames per second (exposure 25ms per image) using a ORCA-Fusion Digital CMOS camera C14440-20UP (Hamamatsu) and HCImageLive software (Hamamatsu). Cells were imaged using an Olympus BX51WI microscope.

Patch-clamp on purified hiPSC-aCM

Voltage-clamp experiments in whole-cell configuration were performed on hiPS-aCM (day 30 of differentiation) at 37°C using a Multiclamp 700B patch-clamp amplifier and a Digidata 1440A (Axon Instruments, Molecular Devices, USA). The ultrarapid delayed rectifier potassium current (I_{Kur}) was recorded as the 4-aminopyridine-sensitive component. To evaluate the current-voltage (IV) relationship, voltage steps of the duration of 300 ms were applied in the range of -50 mV to +50 mV (in -10 mV increments) from a holding potential of -50 mV. The extracellular solution composition was (in mM): 140 NaCl, 5.4 KCl, 1.8 $CaCl_2$, 1 $MgCl_2$. 5 HEPES, 10 Glucose (pH 7.4 with NaOH, 308 mOsm). Borosilicate glass pipettes with a 3-5 MΩ resistance were filled with an intracellular solution containing (in mM): 120 KCl, 20 HEPES, 10 Mg-ATP, 2 $MgCl_2$, 0.2 EGTA-KOH (pH 7.1 with KOH, 290 mOsm). 10 µM nifedipine was added to the extracellular solution to block Ca^{2+} currents; 50 µM 4-aminopyridine added to the extracellular solution and delivered to the cells through a gravity-driven perfusion system. Signals were sampled at 10 kHz and low-pass filtered at 800 Hz. Data are represented as mean±SEM.

Immunofluorescence staining on purified hiPSC-aCM

hiPSC-CMs (day 30 of differentiation) were plated on glass coverslip coated with Matrigel®. After 48h Cells were fixed using PFA 4% for 15 min RT. Three washes of 5 min each at RT in PBS high salt buffer (PBS-HS) were performed. Before antibody staining, the cells were incubated with the permeabilization solution (gelatin 0.4% Triton X-100 0.6%, phosphate buffer 40 mM, NaCl 0.9 M, and saponin 0.1%) for 15 min at RT. Two washes were then conducted with the PBS-HS solution. The non-specific binding sites of the primary antibody were blocked with PBS + 0.5% bovine serum albumin (BSA) + 1% Donckey Serum for 1h at RT. The excess was removed with two 5 min washes in PBS-HS. The primary (Anti-Pro-Atrial Natriuretic Peptide Antibody, clone 11E3.9 mouse monoclonal, Sigma-Aldrich, Catalogue MABC1032; Anti-K_v1.5 Antibody, rabbit polyclonal, alomone labs, Catalogue #APC-004) antibodies were incubated overnight (o/n) at 4 °C and secondary (Donkey Anti-mouse Alexa Fluor 594, Catalogue # A-11005, diluted 1:600; Donkey Anti-rabbit Alexa Fluor 488, Catalogue # A-21206, diluted 1:800, Thermo Fisher Scientific) were incubated for 1 h at RT in the dark, in permeabilization solution. The excess antibodies were then removed with two washes (5 min, RT) in PBS-HS and two washes in PBS low salt (LS). Nuclear Staining was performed with DAPI (10 min RT) and washed in PBS LS. The slides were coverslipped with DAKO fluorescence mounting medium. The Zeiss LSM710 confocal microscope, equipped with a 63× oil immersion objective, was used for image acquisition as a single optical section. Zeiss ZEN Microscope Lite software version and ImageJ 1.48V were used for image processing.

Immunostaining and live cell imaging

NRAMs were fixed with 2% paraformaldehyde for 15 minutes. The cells were washed 3 times with PBS. Cells were then blocked with 10% Donkey serum, 0.3% BSA and 0.1% triton X100 in PBS for 1 hour. Following the removal of the blocking buffer, cells were incubated overnight in 4°C with primary antibody (1:100, LAMP2 (PA1-655)). Cells were then washed 3 times with PBS and incubated in the dark at room temperature (RT) with the secondary antibody goat anti-rabbit IgG conjugated to Alexa Fluor 488 (Molecular probes, Eugene, Ore). Cells were washed 3 times in PBS and coverslips were mounted on slides with Vectashield™ with DAPI to stain the nuclei.

Lysosomes of NRAMs and hiPSC-CMs were labelled with Lysotracker Red (Thermo Fisher Scientific Inc). Cells were washed twice and incubated at RT in the dark for 30 minutes in Tyrode (in mM: NaCl 119, $NaHCO_3$ 25, NaH_2PO_4 1.0, KCl 4.7, $MgCl_2$ 1.2, $CaCl_2$ 1.8, and glucose 10) with 50nM Lysotracker. Cells were washed twice and left in Tyrode for live imaging using Nikon Eclipse Ti Inverted Fluorescence Microscope with a 40x oil-immersion objective with illumination light at 546 nm.

Cells were viewed using a Nikon eclipse Ti inverted confocal microscope (Nikon) with a 63x/1.2 water objective Plan Apo VC 60xA WI DIC N2 lens. NIS-Element viewer (Nikon) was used to acquire multichannel fluorescence images. For detection of DAPI, fluorescence excitation. Excitation at 561

nm was collected at 595nm for detection of AlexaFluor 568nm and imaged sequentially at 2048 × 2048 (12 bits).

Förster resonance energy transfer (FRET)

FRET imaging experiments were performed on day 3 of culture and 24 h after infection of the NRAMs with adenovirus carrying EPAC-S^{H187} cytosolic biosensor [33, 73] at a multiplicity of infection of 1000 virus particles per cell. During experiments, cells were maintained at RT in extracellular (E1) buffer (in mM: NaCl 140, KCl 3, $MgCl_2$ 2, $CaCl_2$ 2, glucose 15, HEPES 10, pH 7.2 with NaOH). Live dynamic measurements were done using an inverted microscope attached to a cool SNAP HQ2 camera and an optical beam splitter (Photometrics) for simultaneous recording of YFP and CFP emissions. FRET changes were measured as changes in the background-subtracted 480nm/545nm fluorescence emission intensity on excitation at 430nm and normalized to the maximum FRET change induced by saturation. For recording, cells were left to stabilize for 4 minutes, drugs, or controls were then added, bafilomycin A1 (100nM), *trans*-Ned-19 (3µM, Insight Biotechnology Ltd) or 0.001% DMSO as a solvent control. 1nM of isoprenaline or 10µM of TPC2-A1-N [34] was then added between 3-6 minutes and left until effect showed a peak and plateau. To induce saturation response of cAMP, FSK (10µM, EMD millipore) to activate ACs and 3-isobutyl-1-methylxanthine (IBMX, 100µM, Sigma-Aldrich) a competitive non-selective phosphodiesterase inhibitor was added.

4pi-SMS imaging

Single molecule localisation microscopy data was acquired from a custom built 4Pi Single Molecule Switching (SMS) microscope [74]. Localisations were accumulated for the LAMP2 structural lysosomal marker throughout the cytosol of a single neonatal rat cardiomyocyte. Fixing and LAMP2 antibody staining of samples were prepared similarly as for immunolabelling (above) and the imaging buffer used was standard GLOX dSTORM imaging buffer. Fixed sample was mounted between two #1.5H x Ø 25 mm coverslips and sealed with two-part silicone adhesive. The raw images were acquired with 10 ms exposure time at 100 frame per second for 10 mins with standard GLOX dSTORM imaging buffer. The power density of 642 nm excitation laser was 7.5 Kw/cm2. The localisations were summed within voxels measuring 16 nm in X and Y and 87.5 nm in Z. The number of localisations within each voxel were resampled to fall within an 8-bit range. Two large dark circular regions visible in the image of the cell (Fig. 4f) are due to fluorescent beads that are laid on top of the cells as fiducial markers for drift correction. These regions have obscured part of the cell volume and thus were cropped out from the reconstructed 3D data. Imaris v10 was used to analyse the image data.

Goat model

The goat model in this study (female C. hircus) is described in [36], where AF was induced and maintained in female goats (C. hircus) for 6 months (AF goat model was created as methodologically described in [75]. Goat were anesthetized and followed by an open chest experiment (N=4 AF and N=4

sham controls) in order to collect tissue and were euthanized. Atrial goat biopsies were either snap frozen or chemically fixed with Karnovsky fixative for electron microscopy studies. The goat study was carried out in accordance with the principles of the Basel declaration and regulations of European directive 2010/63/EU, and the local ethical board for animal experimentation of the Maastricht University approved the protocol.

Human tissue permissions

Tissue used in the research study was obtained from the Royal Papworth Hospital Research Tissue Bank (male patients). Written consent was obtained for all tissue samples using Royal Papworth Hospital Research Tissue Bank's ethical approval (East of England - Cambridge East Research ethics committee). Human right atrial tissue from male patients in sinus rhythm and AF was obtained from the University of Göttingen. Experimental protocols were approved by the ethics committee of the University Medical Center Göttingen (No. 4/11/18). “Biopsies of the atrial appendage were obtained from patients (male and female) undergoing on-pump cardiac surgery at the John Radcliffe Hospital (Oxford, United Kingdom). The study was approved by the Research Ethics Committee (reference no. 07/Q1607/38), and all patients gave written, informed consent.”

Transmission electron microscopy (TEM)

Cardiac tissue was chemically fixed and sectioned using methods described in [24]. Lysosomes were identified by their documented appearance and single lipid bilayer [76]. Analysis and measurements were made using Gatan and ImageJ software.

3D electron tomography

Tomography was performed at two different centre’s in the UK and Germany.

Processing 1) All animal (murine (mixed gender), rabbit (mixed gender), goat (female)) tissue was fixed using iso-osmotic Karnovsky’s fixative (2.4% sodium cacodylate, 0.75% paraformaldehyde, 0.75% glutaraldehyde) as described previously [77]. Semi-thick (300nm) sections were prepared and imaged at the Electron Microscopy Core Facility, European Molecular Biology Laboratory (EMBL) Heidelberg using 300 kV Tecnai TF30 (FEI Company, now Thermo-Fisher Scientific, Eindhoven, The Netherlands) as described previously [78]. Dual-axis tilt series were aligned, reconstructed, and combined using IMOD. Analysis and measurements were made using IMOD and ImageJ software.

Processing 2) Human tissue was fixed in 4% formaldehyde and 2.5% glutaraldehyde in 0.1M sodium cacodylate buffer pH 7.2 for 1 hour at RT ahead of transfer to storage buffer (0.25% glutaraldehyde in buffer). Samples were then rinsed in buffer, treated with 50mM glycine in buffer, rinsed again in buffer and osmicated in 2% osmium tetroxide and 1.5% potassium ferrocyanide in buffer for 1 hour at 4°C with rotation. Samples were then rinsed with MilliQ water and incubated overnight in 0.5% uranyl acetate (aq.). The following day samples were rinsed with MilliQ then dehydrated through an ethanol

series and infiltrated with and embedded in TAAB Hard Plus resin over 3 days. Sections of 250nm were cut from the resin blocks using a Leica UC7 Ultramicrotome and collected onto 3mm copper grids. The sections were then incubated with 10nm gold fiducial markers and post-stained with lead citrate. Tilt series were collected using a JEOL 2100 Plus 200kV TEM equipped with a Gatan OneView camera and reconstructed using IMOD (Etomo).

Rodent isolated cardiomyocyte cytosolic pH measurements

All experiments were performed in accordance with the Home Office Guidance on the operation of The Animals (Scientific Procedures) Act 1986 (H.M.S.O.). Rat ventricular myocytes were isolated according to methods described in [79] and loaded with cSNARF1 in control conditions and in the presence of 1μM bafilomycin A1. Superfusion experiments have been described in detail in [79] and drug was delivered using a rapid switcher device which allowed us to superfuse the cells and alternate between control and drug rapidly, with minimal use of solution.

Tissue sample preparation for proteomics

The right atrial appendage tissue of SR and AF were individually homogenized in a bead homogenizer in RIPA buffer and were reduced using 4X Lithium Dodecyl Sulfate (LDS) buffer and β-mercaptoethanol. Tissue samples were analysed by LC-MS/MS using a Dionex Ultimate 3000 (Thermo Scientific) coupled to a timsTOF Pro (Bruker, [80]) using a 75μm x 150mm C18 column with 1.6μm particles (IonOpticks) at a flow rate of 400nL/minute. A 17- minute linear gradient from 2% buffer B to 30% buffer B (A: 0.1% formic acid in water. B: 0.1% formic acid in acetonitrile) was used. These data are available on PRIDE (Project accession: PXD042391). Atrial tissue contains a range of different cell types from atrial myocytes to vascular smooth muscle cells, endothelial cells, neurons, immune cells and fibroblasts meaning changes in the expression of lysosomal components in specific cell types within the atria in AF cannot be ruled out.

Mass Spectrometry

The TimsTOF Flex (Bruker) was operated in PASEF mode using Compass Hystar 5.0.36.0. Settings for the 11 samples per day method were as follows: Mass Range 100 to 1700m/z, 1/K0 Start 0.6 V·s/cm^2 End 1.6 V·s/cm^2, Ramp time 110.1ms, Lock Duty Cycle to 100%, Capillary Voltage 1600V, Dry Gas 3 l/min, Dry Temp 180°C, PASEF settings: 10 MS/MS scans (total cycle time 1.27sec), charge range 0-5, active exclusion for 0.4 min, Scheduling Target intensity 10000, Intensity threshold 2500, CID collision energy 42eV. Settings for the 50 and 180 samples per day method were as follows: Mass Range 100 to 1700m/z, 1/K0 Start 0.85 V·s/cm^2 End 1.3 V·s/cm^2, Ramp time 100ms, Lock Duty Cycle to 100%, Capillary Voltage 1600V, Dry Gas 3 l/min, Dry Temp 180°C, PASEF settings: 4 MS/MS scans (total cycle time 0.53 sec), charge range 0-5, active exclusion for 0.4 min, Scheduling Target intensity 24000, Intensity threshold 2000, CID collision energy 42eV.

Analysis and statistics on mass spectrometry data

The raw protein intensities of individual SR vs AF group samples were Log transformed and normalised by median subtraction to identify the significantly regulated proteins of interest in AF. The violin plots were created with the InstantClue omics tool version, win-0.12.1 [81]. The protein intensities of the AF vs SR groups were log-transformed and normalized using the Z score. The kernel density estimation of protein intensities for the distribution between groups was represented using a gradient of colour code, red to blue. To study the biological significance, the differentially expressed proteins were subjected to protein network analysis using the Ingenuity Pathway Analysis (IPA) software (Qiagen Inc.) based on curated databases from the literature. IPA is a tool used in omics studies to suggest/predict the effects of specific conditions on biological outcomes. Datasets containing protein identifiers (UniProt) and corresponding expression values (Log2 [Fold change]) of AF vs. sinus rhythm controls were uploaded, and predicted networks were analyzed. Top analysis-ready molecules are found in Supplementary File 3. For visual interpretation, these peptides were input with their FC values into Ingenuity Pathway Analysis (IPA) (Ingenuity Systems, Redwood City, CA) to generate top canonical pathways with color-coded measures of relative FC values (Supplementary Fig. 6c). Figures for canonical pathways were generated in IPA run on 2024-03-21 content version 111725566 with analysis set on Ingenuity Knowledge Base (Genes Only) to include Direct and Indirect relationships.

Statistics

Log[agonist] vs. response (three parameters) was used to form graphs and to calculate EC_{50}s and maximum responses in atrial preparations and are given as mean and (95% confidence interval of best-fit value). Results are presented as the mean ± standard error of the mean (SEM). During a FRET experiments data was collected from individual cells (in one plate) and were averaged to give n=1 and data are represented as n=number of averaged cells per experiments (plate) and N=number of litters used for neonatal isolations (10-14 pups per litter). For FRET analysis, data was normalised and are presented as mean ± SEM of recorded values. datasets were analysed using Kruskal Wallis followed by Dunn's multiple comparison or non-parametric Mann- Whitney U test. Differences were considered statistically significant at values of $P < 0.05$. Statistical significance, when achieved, is indicated as *P<0.05, ** P<0.01, *** P<0.001, **** P<0.0001 and statistical analysis was done using Prism v10 software (GraphPad, CA, USA).

Figure and Legends

Figure 1: Intact spontaneously beating right atrial preparations.

a: Dose-response curves showing changes in beating rate upon cumulative addition of isoprenaline (0.1 to 1000nM) to spontaneously beating murine right atria preparations under control conditions (circles, n=6) and in the presence of either 500nM bafilomycin A1 (diamonds, n=7) or 3µM *trans*-Ned-19 (triangles, n=8). **b**: Table indicating EC_{50} and maximum rate increase measured from dose-response curves in a. **c**: Comparison of spontaneously beating rate in murine right atrial preparations in PSS prior to addition of drug or stimulation with isoprenaline. **d**: Comparison of change in spontaneously beating rate (in %) in murine right atrial preparations in PSS on addition of DMSO, 500nM bafilomycin A1 or 3µM *trans*-Ned-19, prior to stimulation with isoprenaline. **e**: Dose-response curves showing changes in beating rate upon cumulative addition of isoprenaline to spontaneously beating murine right atrial preparations in WT mice (circles, n=9) and in $TPC2^{-/-}$ mice (squares, n=9). Asterisks indicate significance level for effect of bafilomycin A1 and *trans*-Ned-19 compared to control; *p<0.05; **p<0.01.

Figure 2: Sino-atrial node single cell data in guinea pig.

a: Brightfield image of live isolated guinea pig SAN myocyte. **b**: Representative traces showing spontaneously generated Ca^{2+} transients in an isolated SAN myocyte in the presence of DMSO and after exposure to 3nM isoprenaline. **c**: Representative traces to show spontaneously generated Ca^{2+} transients in an isolated SAN myocyte in the presence of 100nM bafilomycin A1 and after exposure to 3nM isoprenaline. **d**: Beating rate of SAN myocytes in the presence of either DMSO or 100nM bafilomycin A1. **e**: Maximum change in beating rate response (in %) of SAN myocytes in the presence of either DMSO or bafilomycin A1 after exposure of 3nM isoprenaline. **f**: Change in the beating rate response (in %) of SAN myocytes in the presence of either DMSO or 100nM bafilomycin A1 after exposure of 3nM isoprenaline over 4 minutes. **g**: Ca^{2+} transient amplitude of SAN myocytes in the presence of either DMSO or bafilomycin A1 in PSS. **h**: Maximum change in Ca^{2+} transient amplitude response (in %) of SAN myocytes in the presence of either DMSO or 100nM Bafilomycin A1 after exposure of 3nM isoprenaline. **i**: Change in Ca^{2+} transient amplitude response (in %) of SAN myocytes in the presence of either DMSO or bafilomycin A1 after exposure of 3nM isoprenaline over 4 minutes. ns=non-significant, *P<0.05.

Figure 3: Measurement of calcium transients in hiPSC-CM.

a: Snapshots of hiPSC-CM loaded with Fluo-5F-AM. **b**: Representative traces showing spontaneously generated Ca^{2+} transients in hiPSC-CM in the presence of a solvent control DMSO and after exposure to 3nM isoprenaline. **c**: Representative traces showing spontaneously generated Ca^{2+} transients in isolated hiPSC-CM in the presence of 100nM bafilomycin A1 and after exposure to 3nM isoprenaline. **d**: Beating rate of hiPSC-CM-CMs in the presence of either DMSO (n=14, N=4) or 100nM bafilomycin

A1 (n=11, N=3) in PSS. **e**: Change in beating rate response (in%) of hiPSC-CM myocyte in the presence of either DMSO (n=14, N=4) or 100 nM bafilomycin A1 (n=11, N=3) after exposure of 3nM isoprenaline over 4 minutes. **f**: Ca^{2+} transient amplitude of hiPSC-CM in the presence of either DMSO (n=14, N=4) or 100nM bafilomycin A1 (n=11, N=3) in PSS. **g**: Change in Ca^{2+} transient amplitude response (in %) of hiPSC-CM in the presence of either DMSO (n=14, N=4) or 100nM bafilomycin A1 (n=11, N=3) after exposure of 3nM isoprenaline over 4 minutes. ns=non-significant, **P<0.01, ***P<0.001, ****P<0.0001.

Figure 4: Measuring cAMP levels in response to isoprenaline in neonatal rat atrial myocytes (NRAMs).

a: Image showing representative staining in NRAMs for LAMP2. **b**: 4Pi-SMS super-resolution microscopy analysis. Visualisation Z-projection of the 4Pi SMS image data indicating lysosomes (spheres) which are less than (yellow) or more than [82] 500 nm of their nearest neighbour. Scale bar 2 µm. **c**: Representative image of EPAC-S^{H187} FRET biosensors in NRAMs. **d**: Quantification of the peak FRET change in response to 1nM isoprenaline in NRAMs the presence of either DMSO (n=11, N=5) or 100nM bafilomycin A1 (n=4, N=4) in E1 buffer. **e**: Quantification of the peak FRET change in response to 1nM isoprenaline in NRAMs in the presence of either DMSO (n=4, N=4) or 100nM bafilomycin A1 (n=4, N=4) in 0 Ca^{2+} E1 buffer. **f**: Quantification of the peak FRET change in response to 1nM isoprenaline in NRAMS pre-incubated at 37 °C for 45 minutes with 2 µM thapsigargin and 2µM ryanodine in the presence of either DMSO (n=6, N=5) or 100nM bafilomycin A1 (n=7, N=5) in 0 Ca^{2+} E1 buffer. **g:** Live representative images of hiPSC-aCM labelled with lysotracker. **h:** Quantification of the peak FRET change in response to 1nM isoprenaline in hiPSC-aCM myocytes in the presence of either DMSO (n=7, N=4) or 100nM bafilomycin A1 (n=8, N=3). ns=non-significant, *P<0.05, **P<0.01, ***P<0.001, ****P<0.0001.

Figure 5 (related to Figure 4): AC1 and CAMKII study.

a: Quantification of the peak FRET change in response to 10µM TPC2-A1-N in NRAMs in the presence of either DMSO in E1 buffer (n=7, N=5) or pre-incubated at 37 °C for 45 minutes with 2µM thapsigargin and 2µM ryanodine in 0 Ca^{2+} E1 buffer (n=5, N=5), 100nM bafilomycin A1 (n=6, N=4) or 1µM *trans*-Ned-19 (n=6, N=4) in E1 buffer. **b:** Quantification of the peak FRET change in response to 10µM TPC2-A1-N in NRAMs in the presence of either DMSO in E1 buffer (n=7, N=5) or pre-incubated at 37 °C for 45 minutes with 2µM thapsigargin and 2µM ryanodine in 0 Ca^{2+} E1 buffer (n=5, N=5), 3µM ST034307 (n=4, N=4) or 1µM KN-93 (n=4, N=4) in E1 buffer. **c:** Isolated, fixed, and immunohistochemistry-stained representative image of Guinea pig SAN myocyte with LAMP2(**i**, green), AC1 (**ii**, red) and merged image (**iii**, using imageJ).

Figure 6: Spatial interaction between lysosome-sarcoplasmic reticulum and lysosome-mitochondria.

a: Histogram showing the distribution of lysosome-SR and lysosome-mitochondria distance found in rabbit atria. **b.** Electron microscopy image of a lysosome (Ly) in close proximity to sarcoplasmic reticulum [1] and mitochondria in rabbit atria. **c.** Maximum lysosomal diameter in nanometers (nm) measured in rabbit atria. **d.** Shortest distance measured between lysosomes-SR (n=13) and lysosome-mitochondria (n=11) analysed from transmission electron microscopy images of rabbit atrial tissue. **e-f:** Representative 3D electron tomography images of murine SAN including raw images (e and f top panels) and reconstructed organelles in 3D (e and f bottom panels) of lysosomes (red), sarcoplasmic reticulum (blue) and mitochondria (yellow)**. Model lysosomes (Ly, red), sarcoplasmic reticulum (SR, blue), mitochondria (M, yellow).**

Figure 7: Lysosome size and positioning quantification in goat AF tissue using electron microscopy.

a: Maximum lysosomal diameter in sham-operated (286.2±17.2nm, N=4 goats, n=37 lysosomes) and AF goats (479.1±54.3nm, N=4 goats, n=18 lysosomes). **b**: Minimum distance between lysosomes and nearest SR measured in sham-operated (14.11±1.5nm, N=4 goats, n=37 lysosomes) and AF goats (19.45±1.9nm, N=4 goats, n=18 lysosomes). **c**: Minimum distance between lysosomes and mitochondria in sham-operated (185.5±31.9nm, N=4 goats, n=37 lysosomes) and AF goats (74.9±17.6nm, N=4 goats, n=18 lysosomes). **d-e:** Representative electron tomography raw images from sham-operated (**d top panel**) and AF (**e top panel**) goats and the 3D electron tomography reconstructed organelles in (d and 3 bottom panels). Lysosomes (Ly-red), mitochondria (Mito-yellow) and SR (SR-blue). *P<0.05, **P<0.01.

Figure 8: Proposed simplified model of NAADP mediated Ca^{2+} release in atrial myocytes and influence atrial cardiac function and pacemaking in response to β-adrenergic response.

a: Representative scheme of proposed mechanisms by which activation of β-AR by isoprenaline lead to ACs activation (AC4 and 5) leading to activation of PKA by cAMP and synthesis of NAADP by CD38 enhancing lysosomal Ca^{2+} release by the action of NAADP on lysosomal TPC2 channels, located in proximity, a few nanometres. **b**: Simplified flowchart of proposed mechanism of action upon β-adrenergic stimulation. Image created with Biorender.com.

FIGURES

Figure 1:

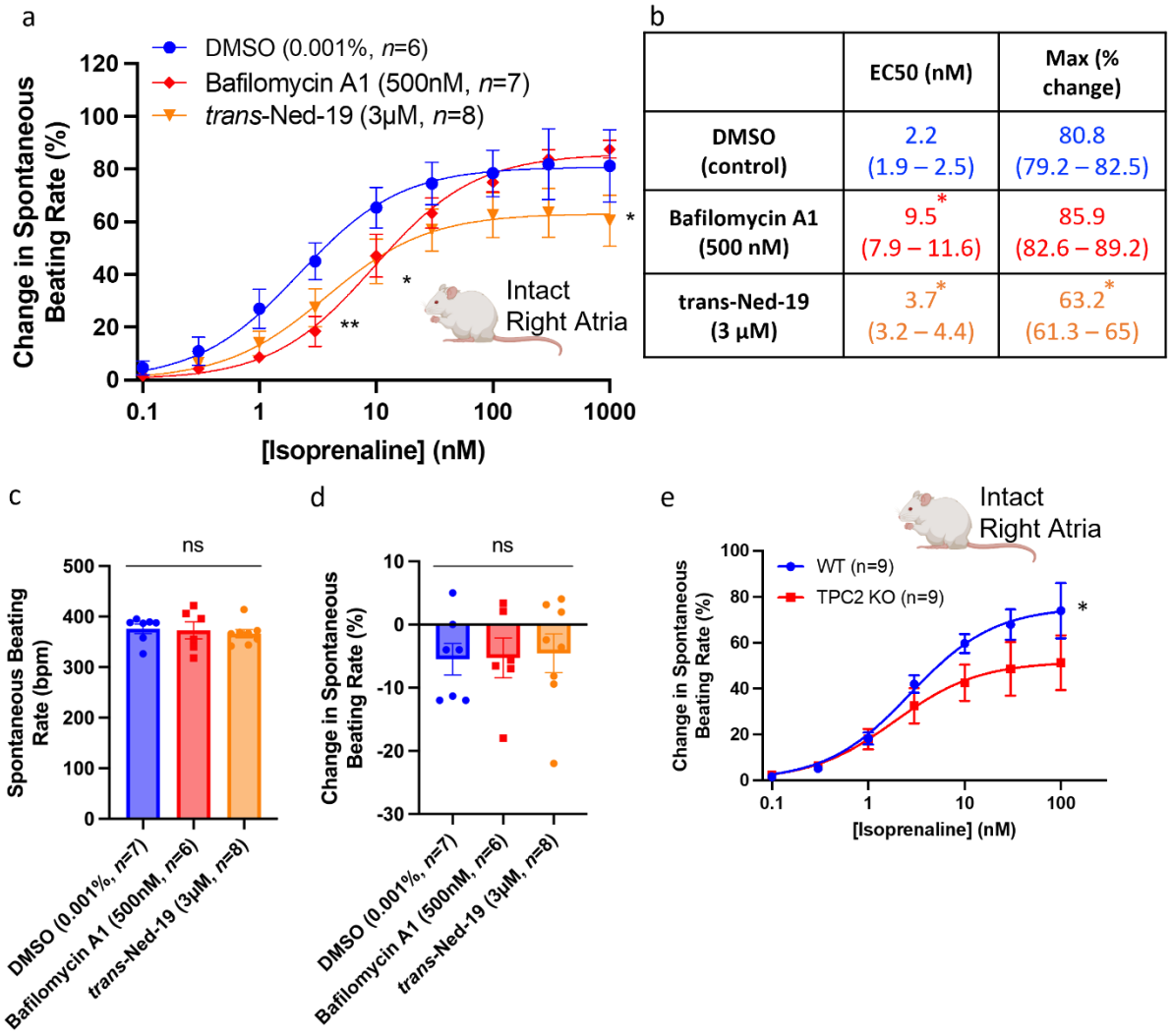

	EC50 (nM)	Max (% change)
DMSO (control)	2.2 (1.9 – 2.5)	80.8 (79.2 – 82.5)
Bafilomycin A1 (500 nM)	9.5* (7.9 – 11.6)	85.9 (82.6 – 89.2)
trans-Ned-19 (3 μM)	3.7* (3.2 – 4.4)	63.2* (61.3 – 65)

Figure 2:

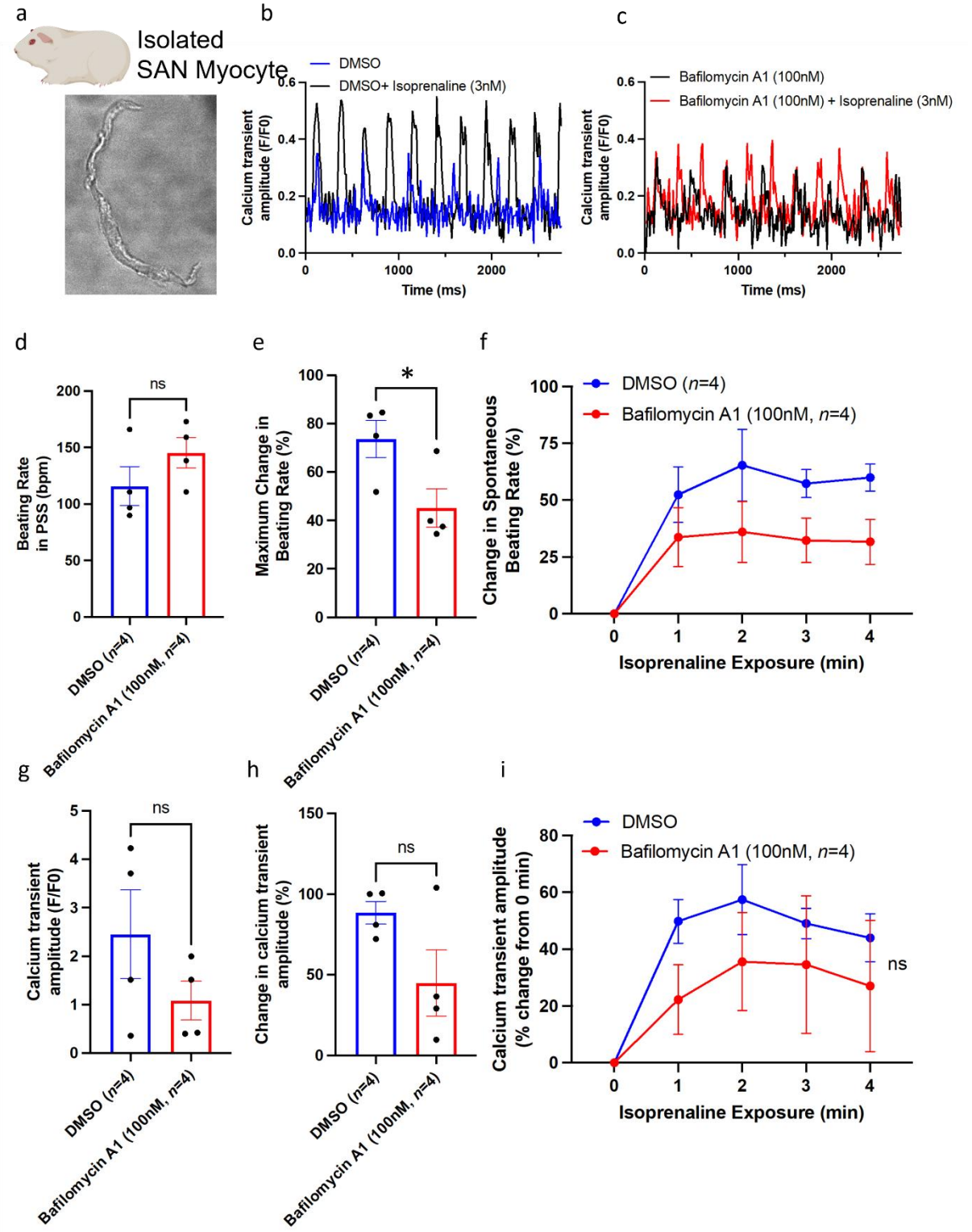

Figure 3:

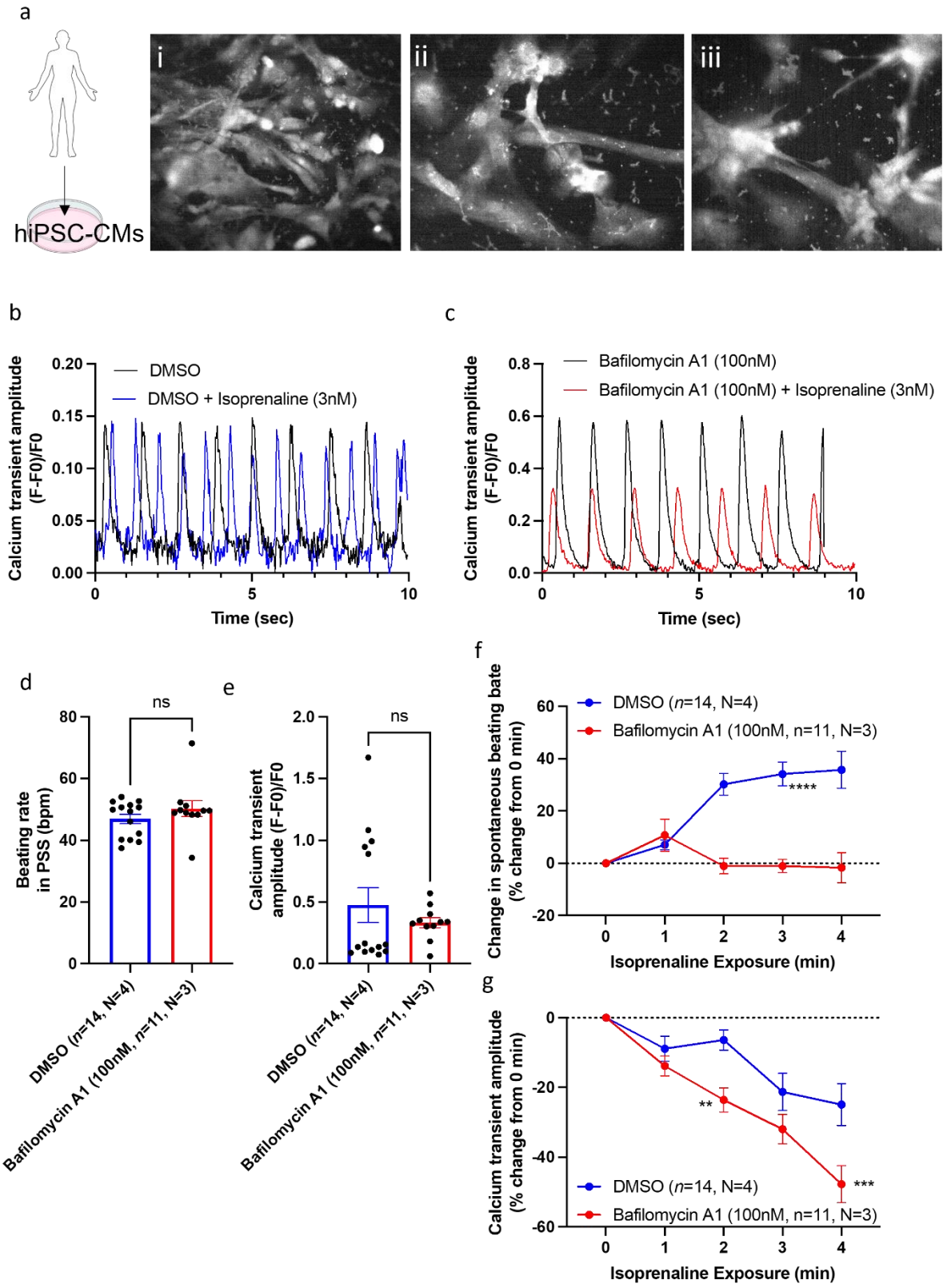

Figure 4:

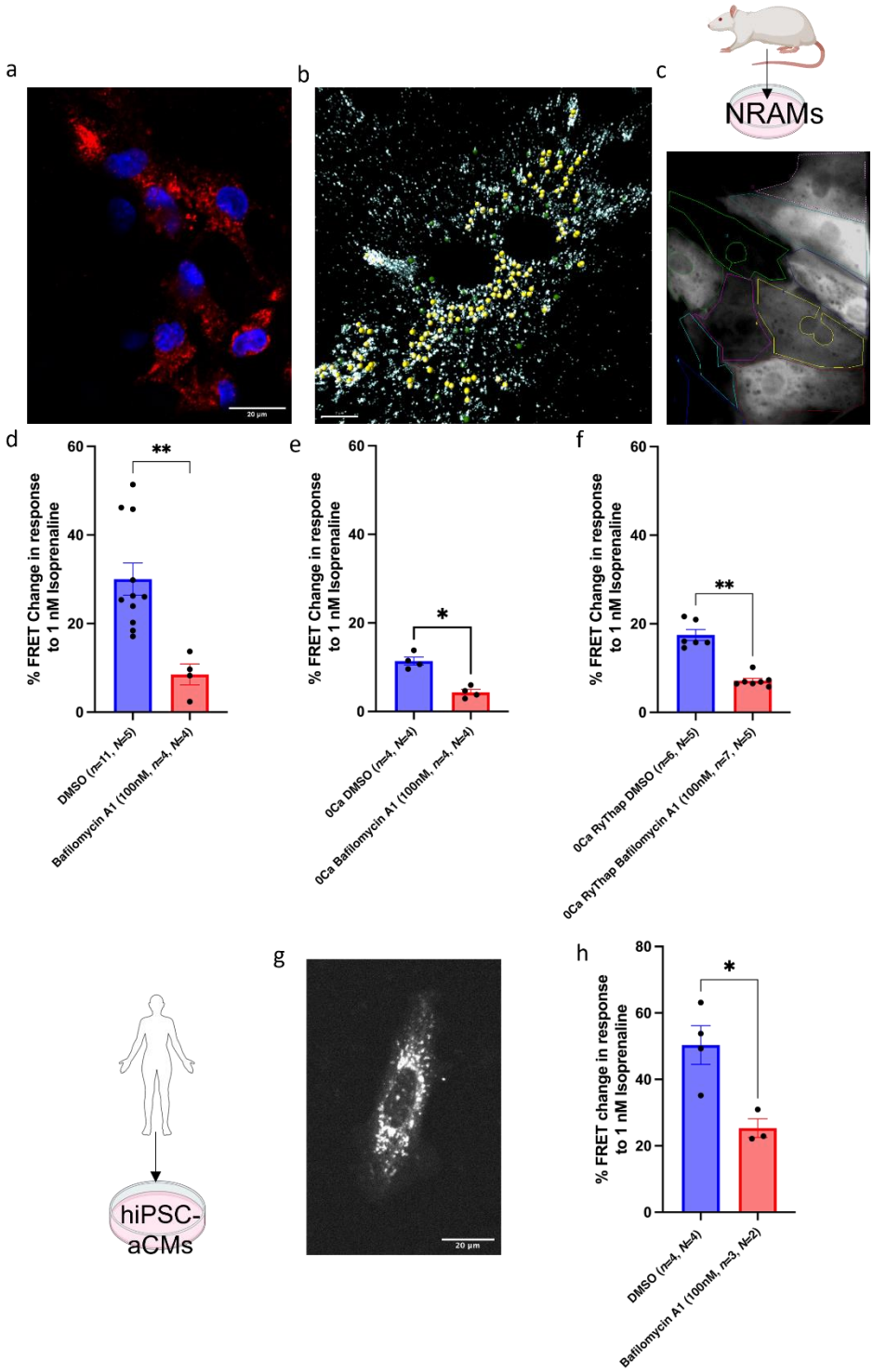

Figure 5:

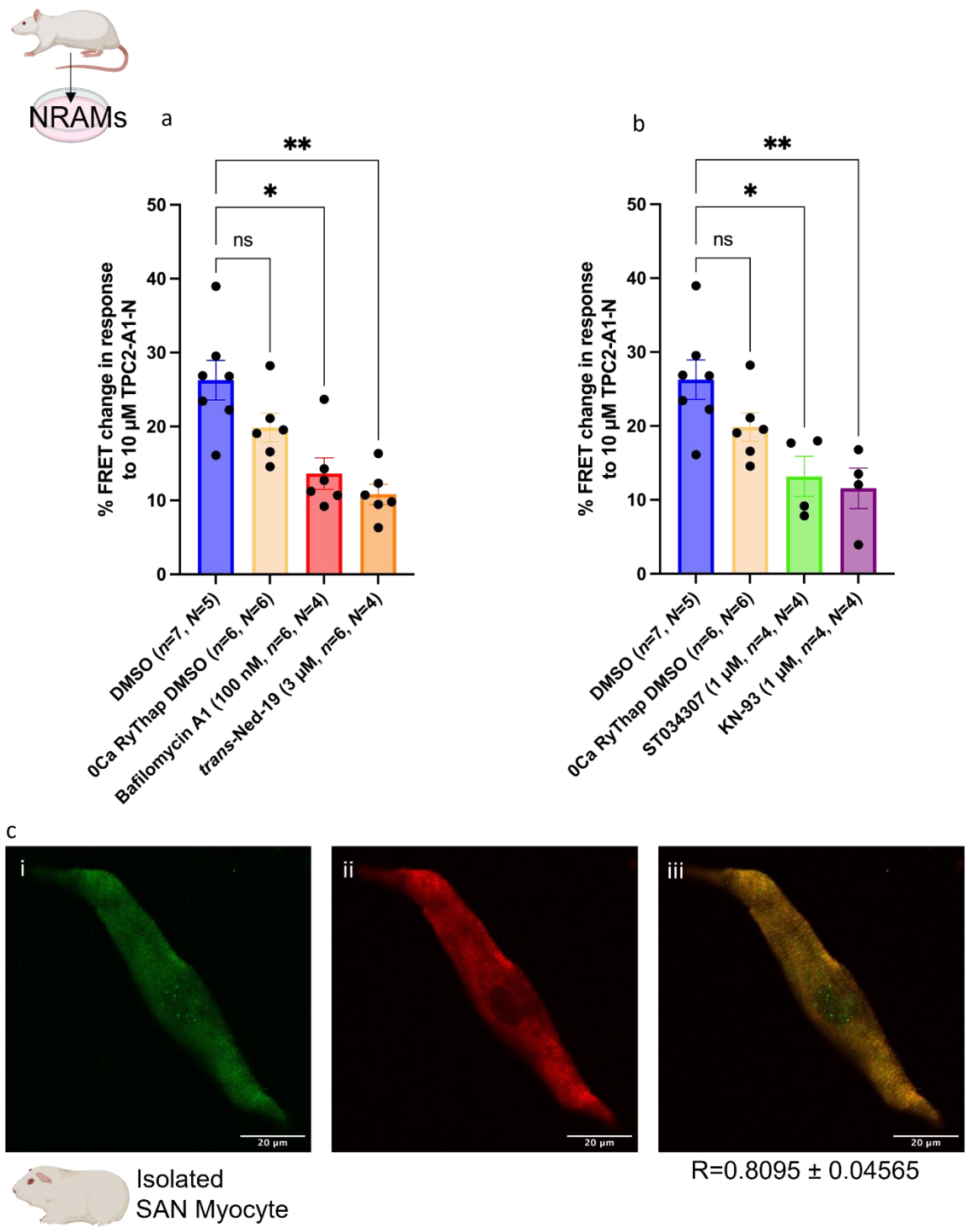

Figure 6:

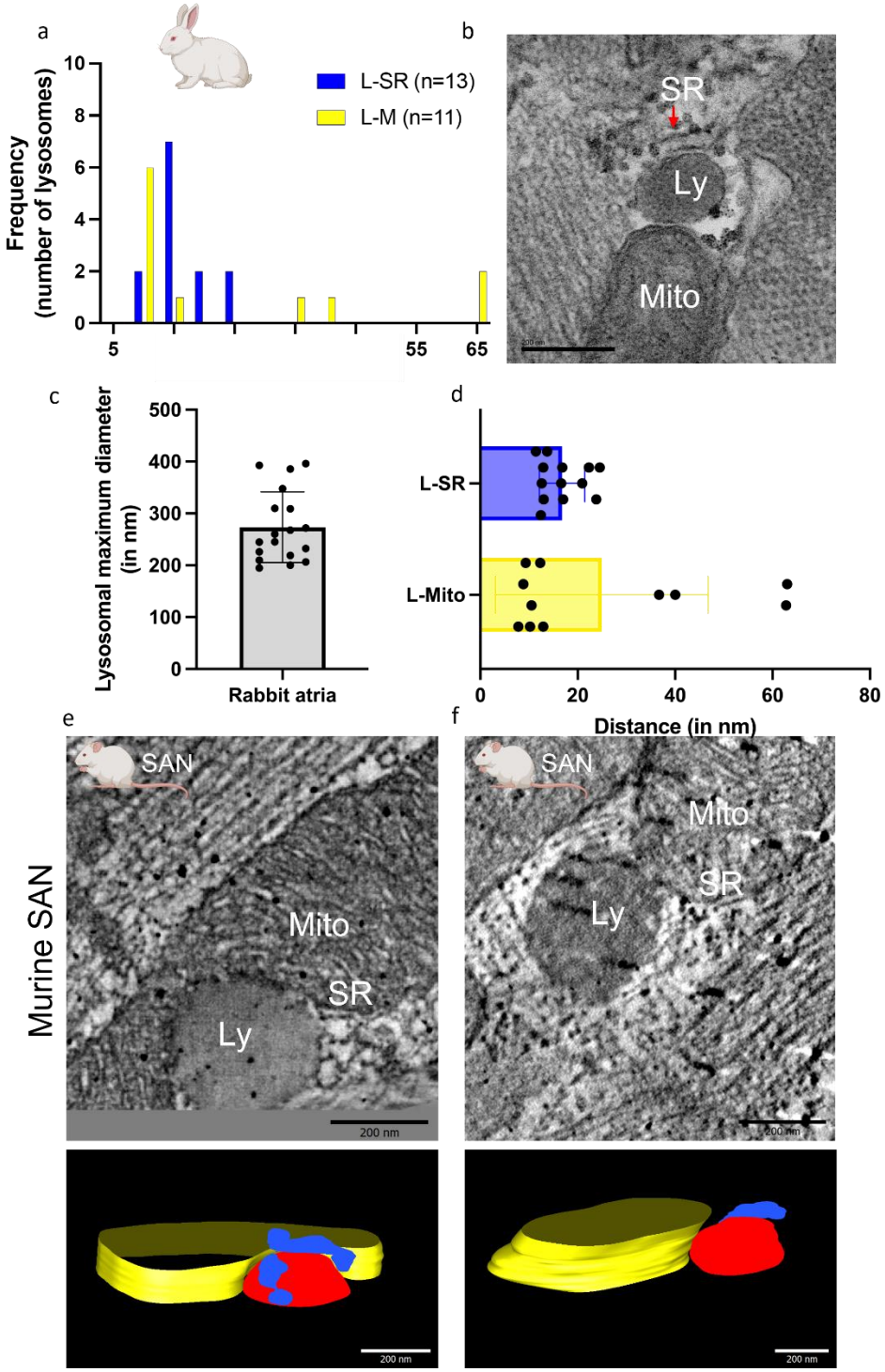

Figure 7:

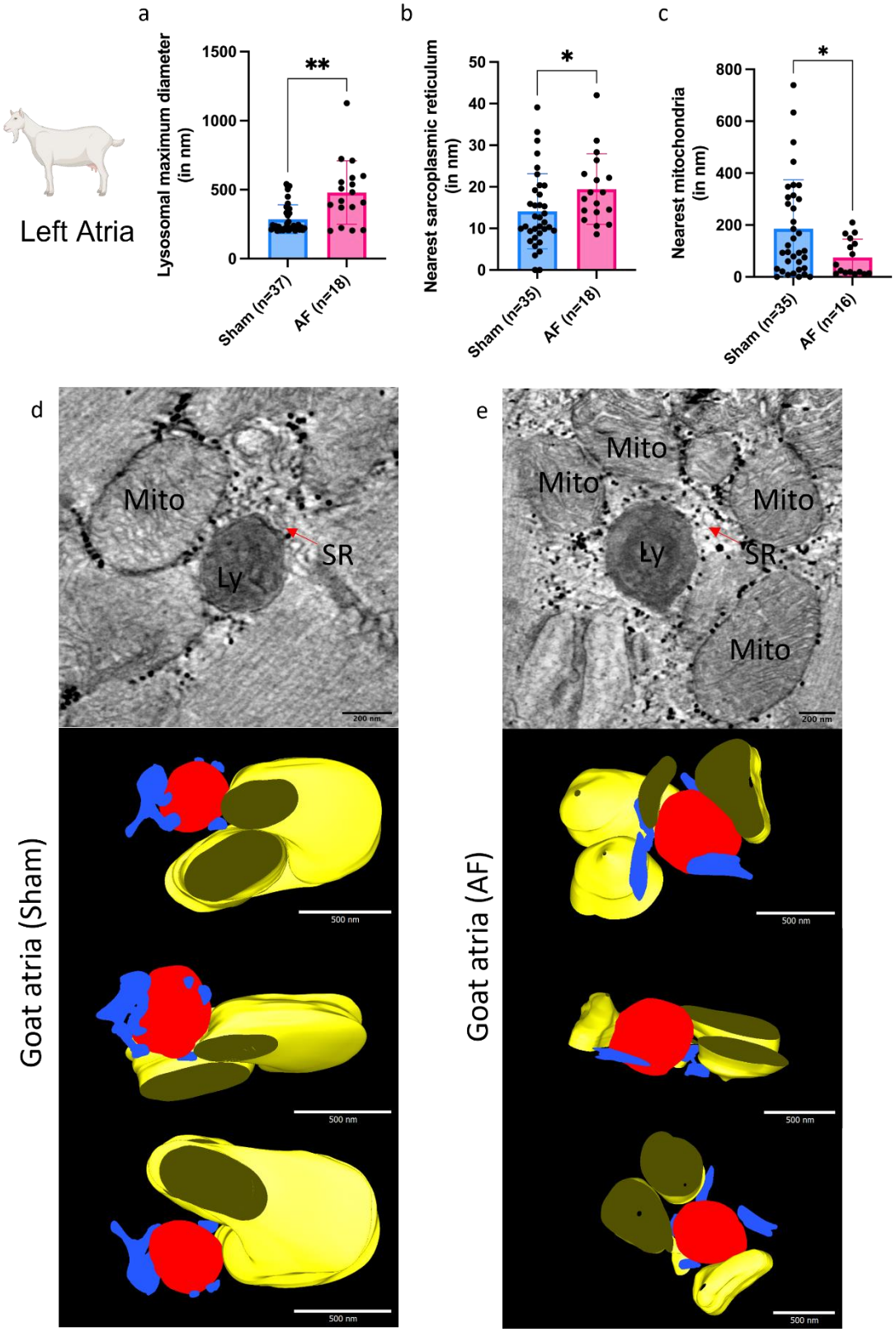

Figure 8:

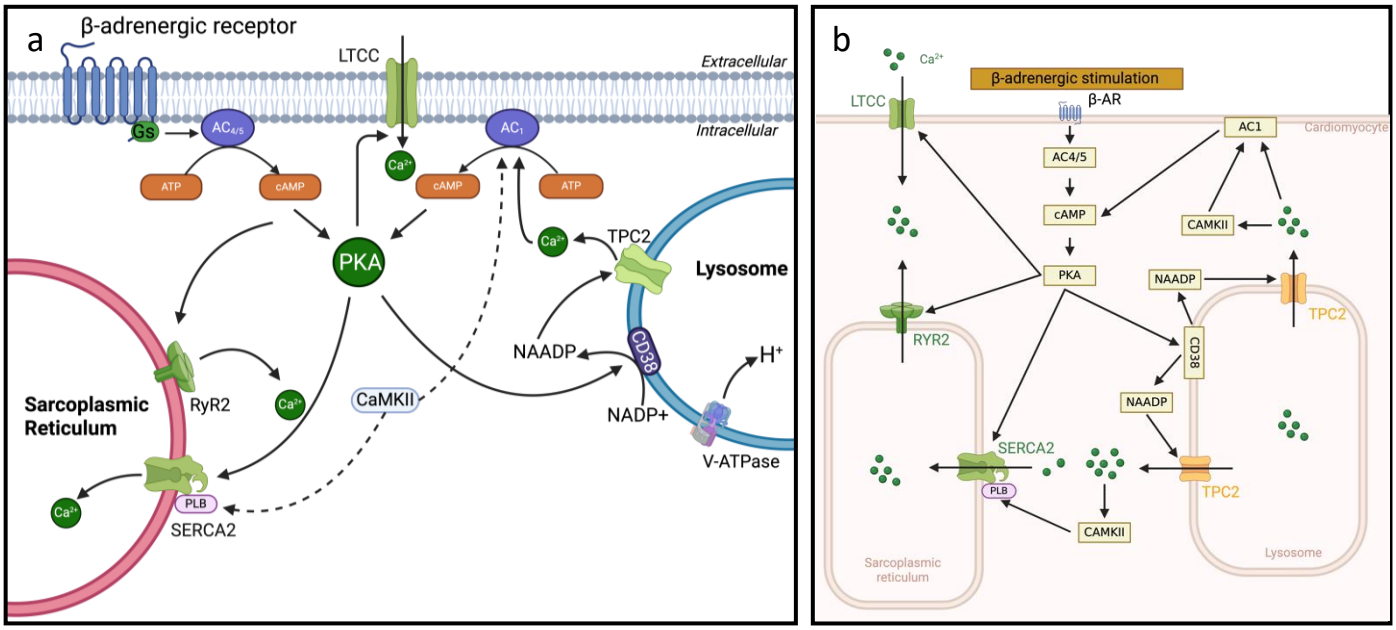

Supplement Figure Legends

Supplementary Figure 1 (related to figure 1): Left atrial force transducer experiments. a: Dose-response curves to show change in tension generated on cumulative addition of isoprenaline to stimulated (5Hz) murine left atria preparations under control conditions (circles, n=7) and in the presence of either 100nM bafilomycin A1 (diamonds, n=9) or 3µM *trans*-Ned-19 (triangles, n=6). **b**: Comparison of tension force in beating murine left atrial preparations in PSS prior to addition of drug or stimulation with isoprenaline. **c**: Comparison of change in beating force (in %) in beating murine left atrial preparations in PSS on addition of DMSO, 100nM bafilomycin A1 or 3µM *trans*-Ned-19, prior to stimulation with isoprenaline. **d**: Dose-response curves to show change in tension generated on cumulative addition of isoprenaline to stimulated (5Hz) murine left atria preparations in WT mice (circles, n=11) and in TPC2$^{-/-}$ mice (squares, n=11).

Supplementary Figure 2 (related to figure 4e): 4Pi-SMS super-resolution microscopy analysis. a: Visualisation of the 4Pi SMS image data [83] indicating lysosomes (spheres) which are less than (yellow) or more than [82] 500 nm of their nearest neighbour. **b**: Distribution of nearest neighbour distances. **c**: Spectrum of measured lysosome volumes.

Supplementary Figure 3 (related to figure 4): characterization of hiPS-aCM. a: Representative sample traces of potassium currents elicited at +50mV in control (black) or in the presence of 50µM 4-AP in hiPS-aCM (i) and in hiPS-CMs (ii). **b**: Current-voltage relationships of 4-AP-sensitive currents in hiPS-aCM and in hiPS-CMs (n= number of cells, N=number of independent differentiations) **c:** Image showing representative staining in hiPSC-aCM; the plasma membrane localization of K_v1.5 (i, green), nuclear Staining DAPI (ii, blue), and merge image (iii, using ImageJ)**. d:** Image showing representative staining in hiPSC-aCM of pro-ANP localization in perinuclear region e cytosolic granuli (i, red), nuclear Staining DAPI (ii, blue), and merge image (iii, using ImageJ)**.** Scale bar 20µm.

Supplementary Figure 4 (related to figure 6): Goat left atrial electron microscopy. Snap shots from goat left atrial sinus rhythm control (column **a**) and atrial fibrillation (column **b**) from 3D tomograms to show proximity of Lysosomes (Ly) to Mitochondria [84] and Sarcoplasmic Reticulum [1]. Scale bars provided on each image.

Supplementary Figure 5 (related to figure 2): Rodent isolated cardiomyocyte cytosolic pH measurements. a: Rat ventricular myocytes, loaded with cSNARF1 in control condition and in the presence of 1µM bafilomycin A1. **b**: Rat ventricular myocytes, loaded with cSNARF1 and measured in HEPES buffer extracellular solution (in mM: NaCl 130, KCl 4.5, HEPES 20, $CaCl_2$ 1, $MgCl_2$ 1, Glucose 11) exposed to 1µM bafilomycin A1 by dual microperfusion (n=8).

Supplementary Figure 6 (related to discussion): IPA analysis of human tissue samples. a: Violin Plot of protein intensity preparations in right atrial appendage human samples from atrial fibrillation patient (N=6) and patient with a normal sinus rhythm (N=7). **B:** Volcano Plot of differential gene

expression of human samples from atrial fibrillation patient (N=6) and patient with a normal sinus rhythm (N=7), MaxLFQ is a generic method for label-free quantification, proteins with fold changes greater than 2 are highlighted, Instant Clue v0.12.1. See Supplementary File 1 for protein list. **c:** The highest ranked canonical IPA pathways of the differentially expressed proteins (using a score cut off -log (p values) are greater than 3.8). The horizontal axis shows the pathway names and the vertical axis is the p-value (-log) of each pathway. Blue bars: negative z-score; orange bars: positive z-score and clear bars are indicative of a z-score of 0, and thus have no difference in activity. Grey shaded bars indicate that there is no activity pattern available identified by IPA, despite highly significant association of the proteins within the pathway. See Supplementary File 2 for list.

Supplementary Figure 7 (related to discussion): Pathway analysis of human tissue samples. a: Pathways analysis in IPA; Bubble plot showing top canonical pathways when comparing AF with sinus rhythm control samples. The intensity of the colour depicts the relative increase (red) or decrease [82] in protein counts with the size of the bubble representing the number of proteins found in the pathway. **b:** Integrin Signalling Pathway showing in colour all proteins found within the dataset. Red represents upregulation in AF. Whereas Green depicts down regulation **c,** Microautophagy top Canonical Pathway showing in colour all proteins found within the dataset. Red represents upregulation in AF. **d:** Plot of differentially expressed proteins (p= 1.98E-05) from the microautophagy regulation pathway showing how each protein changes with AF.

Supplementary Figure 8 (related to discussion): Top 10 networks analysed in IPA. **a**: Cell-To-Cell Signaling and Interaction, Cellular Assembly and Organization, Cellular Function and Maintenance; **b**: Cell Cycle, Infectious Diseases, Organismal Injury and Abnormalities; **c**: Developmental Disorder, Hematological Disease, Hereditary Disorder; **d**: Cell Morphology, Neurological Disease, Organismal Injury and Abnormalities; **e**: Connective Tissue Disorders, Dermatological Diseases and Conditions, Developmental Disorder; **f**: Energy Production, Nucleic Acid Metabolism, Small Molecule Biochemistry; **g**: Cardiac Arrythmia, Cardiovascular Disease, Hereditary Disorder. List of regulated proteins used in IPA can be found in Supplementary File 2 and Supplementary File 3 contains Ingenuity Canonical Pathways Analysis which includes molecules.

Supplementary Figure 9 (related to discussion): The top regulator effects and interaction networks mapped by IPA. a: CALR, DNMT3A, ESRRA (consistency score of 1.152). **b**: ESRRG (consistency score of 0.577). **c**: MMP9 (consistency score of -6.0).

Supplementary Figure 10 (related to discussion): Lysosome size and positioning in human atrial tissue from patients in sinus rhythm and atrial fibrillation using 2D transmission EM tile scans. a: Quantification of the area occupied by lysosomes in a defined cell area (dotted yellow lines define the cell area chosen (seen in d-g)) in sinus rhythm (SinusR) tissue (0.2538±0.028%, N=1 patient, n=10 cells) and in AF tissue (0.4851±0.035%, N=1 patient, n=13 cells). **b**: Lysosomal maximal diameter in SinusR tissue (260±3.1nm, N=1 patient, n=194 lysosomes) and in AF tissue (313±3.3nm, N=1 patient,

n=392 lysosomes). **c**: Distance between lysosomes and SR in SinusR tissue (17.93±0.7nm, N=1 patient, n=63 measurement) and in AF tissue (28.99±0.4nm, N=1 patient, n=129 measurements). **d**: Representative images (large overviews and zoomed-in insets) of lysosomes and SR in patient with SinusR. **e**: Representative images (large overviews and zoomed-in insets) of lysosomes and SR in patient with AF. Statistical analysis was not possible due to a low patient number. Scale bar represents 2μm.

Supplementary Figure 11 (related to discussion): Lysosomes are in close proximity to sarcoplasmic reticulum and mitochondria in human adult atrial cardiomyocytes, feasibly forming nanojunctions. Top Image: Representative example of lysosome (Ly) in contact with mitochondria [84] and in close proximity to sarcoplasmic reticulum [1] and mitochondria [84] in human left atrial tissue section. **Bottom Image:** zoomed area of the black circle in the top image.

Supplementary Files:

Supplementary File 1 (related to discussion, student T-test): Volcano Plot excel output file. Used to determine significant data points in a data set with a permutation-based FDR, X- axis column displays: log2 fold changes and Y- axis column displays: -log10 p values. Column headers are gene/protein description and columns labelled with the sample IDs are showing the mass spectrometry signal intensities in log2, normalized by MaxLFQ [85].

Supplementary File 2 (related to discussion): List of significant up and down regulated proteins taken from supplementary file 1 for analysis in IPA.

Supplementary File 3 (related to discussion): Canonical Pathways Analysis in IPA.

Supplementary Videos:

Supplemental Video 1 (related to Figure 6): Mouse Sino-Atrial Node tissue. 3D animation of tomographic reconstruction of cell in Fig. 6e-f. Red: Lysosome, Blue: Sarcoplasmic reticulum, Yellow: Mitochondria.

Supplemental Video 2 (related to Figure 7): Left atrial goat tissue (sham control). 3D animation of tomographic reconstruction of cell in Fig. 7d. Red: Lysosome, Blue: Sarcoplasmic reticulum, Yellow: Mitochondria.

Supplemental Video 3 (related to Figure 7): Left atrial AF goat tissue (atrial fibrillation). 3D animation of tomographic reconstruction of cell in Fig. 7e. Red: Lysosome, Blue: Sarcoplasmic reticulum, Yellow: Mitochondria.

Supplemental Video 4 (related to discussion): A simple segmented video using iMovie and Keynote (IOS software) of a lysosome in close proximity to sarcoplasmic reticulum and mitochondria from human left atrial tomogram. Lysosome (red) in contact with mitochondria (yellow) and in close proximity to sarcoplasmic reticulum (blue) in human left atrial tissue.

SUPPLEMENTARY FIGURES

Supplementary Figure 1:

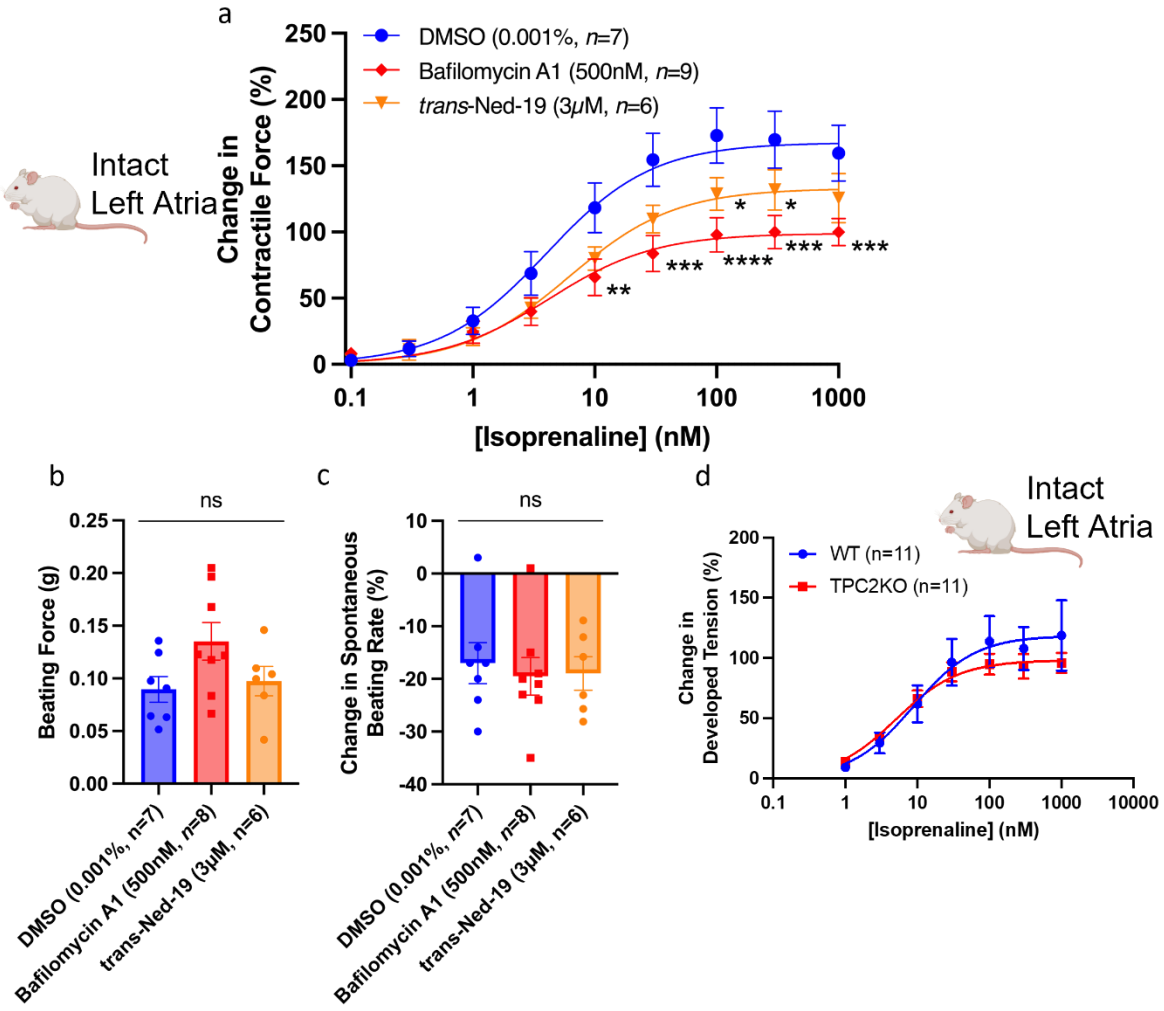

Supplementary Figure 2:

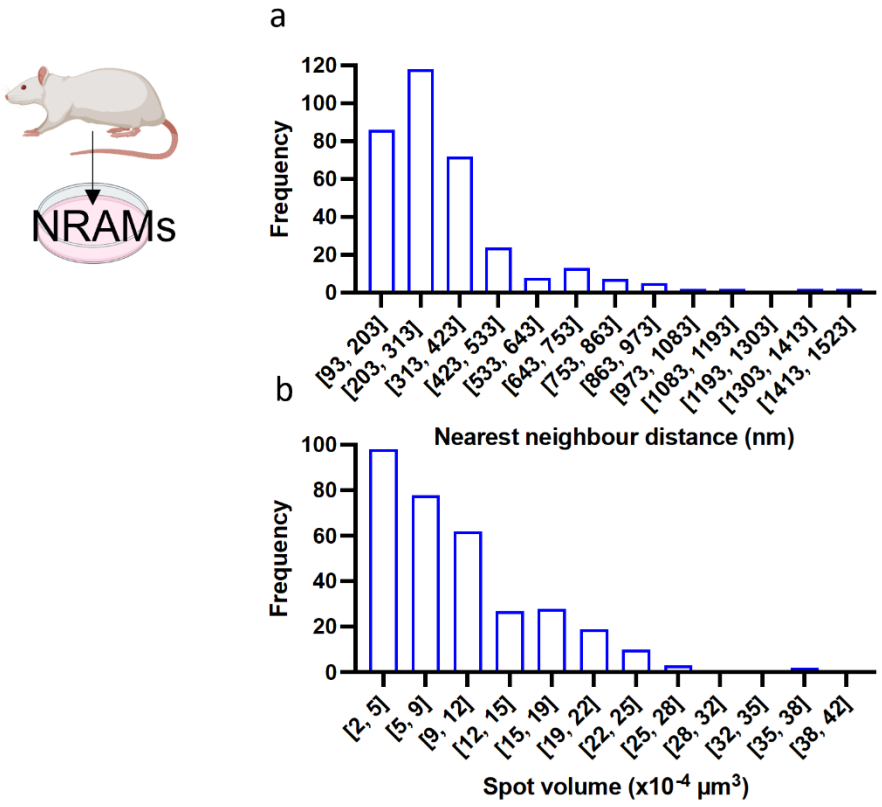

Supplementary Figure 3:

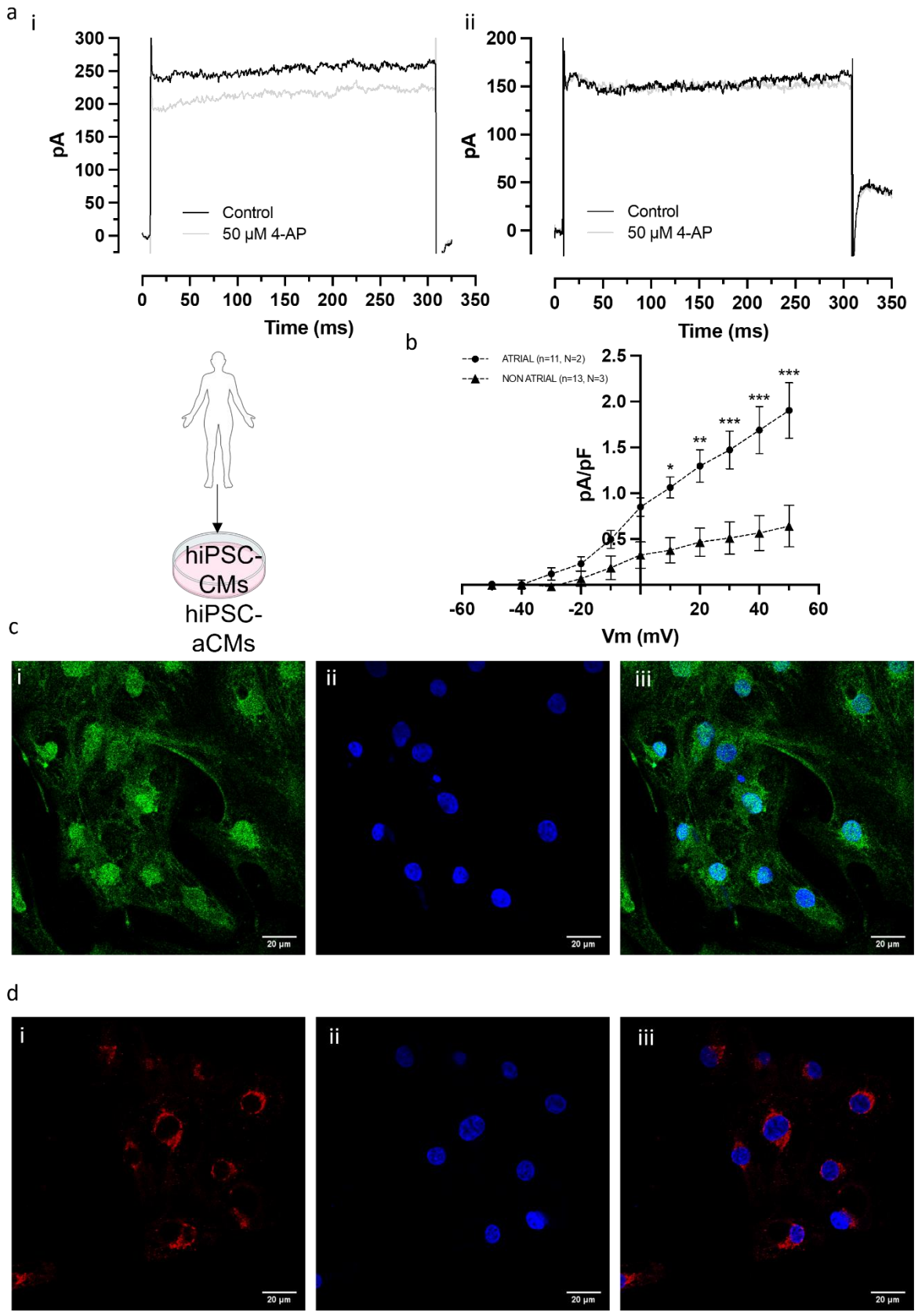

Supplementary Figure 4:

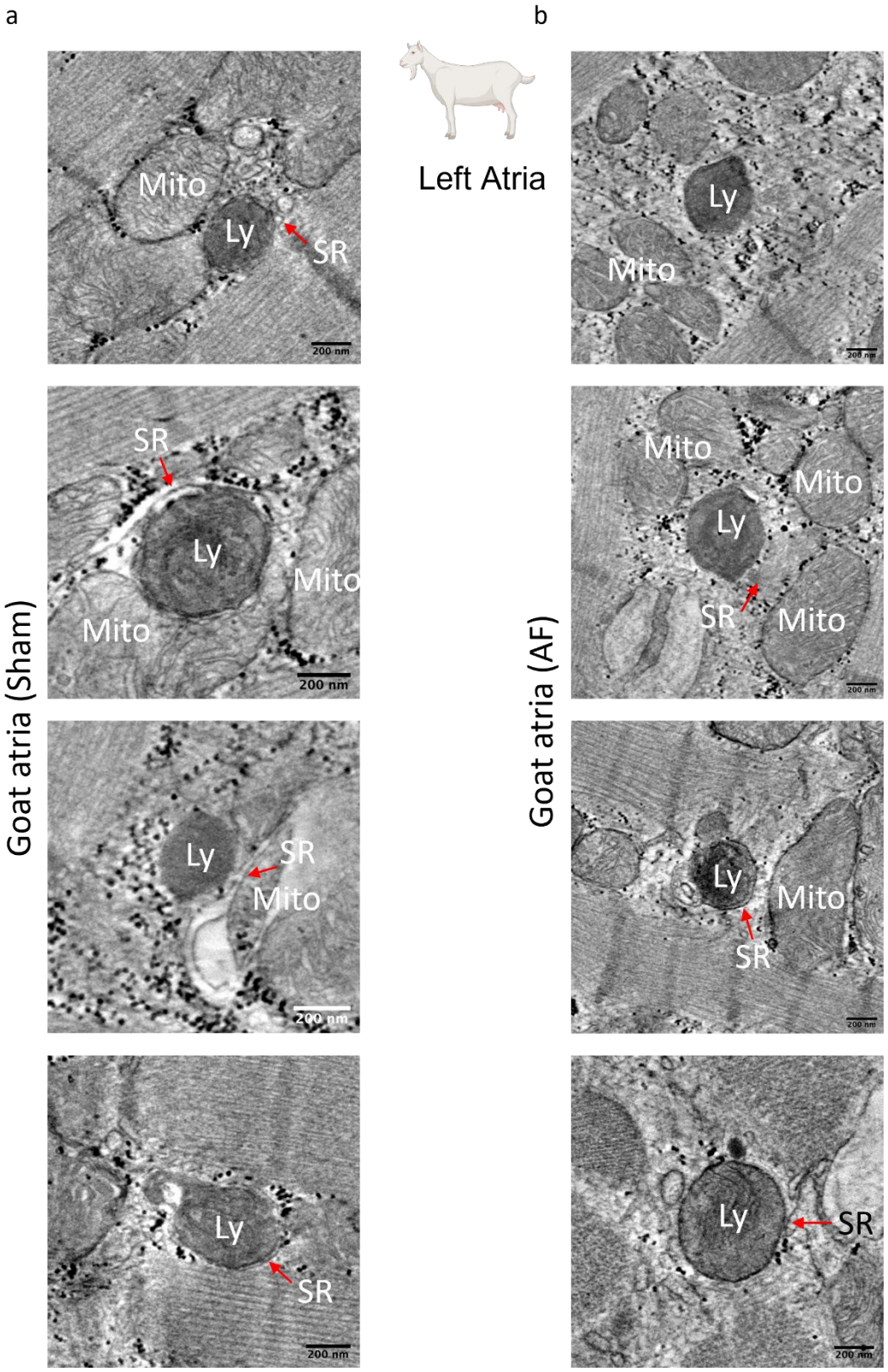

Supplementary Figure 5:

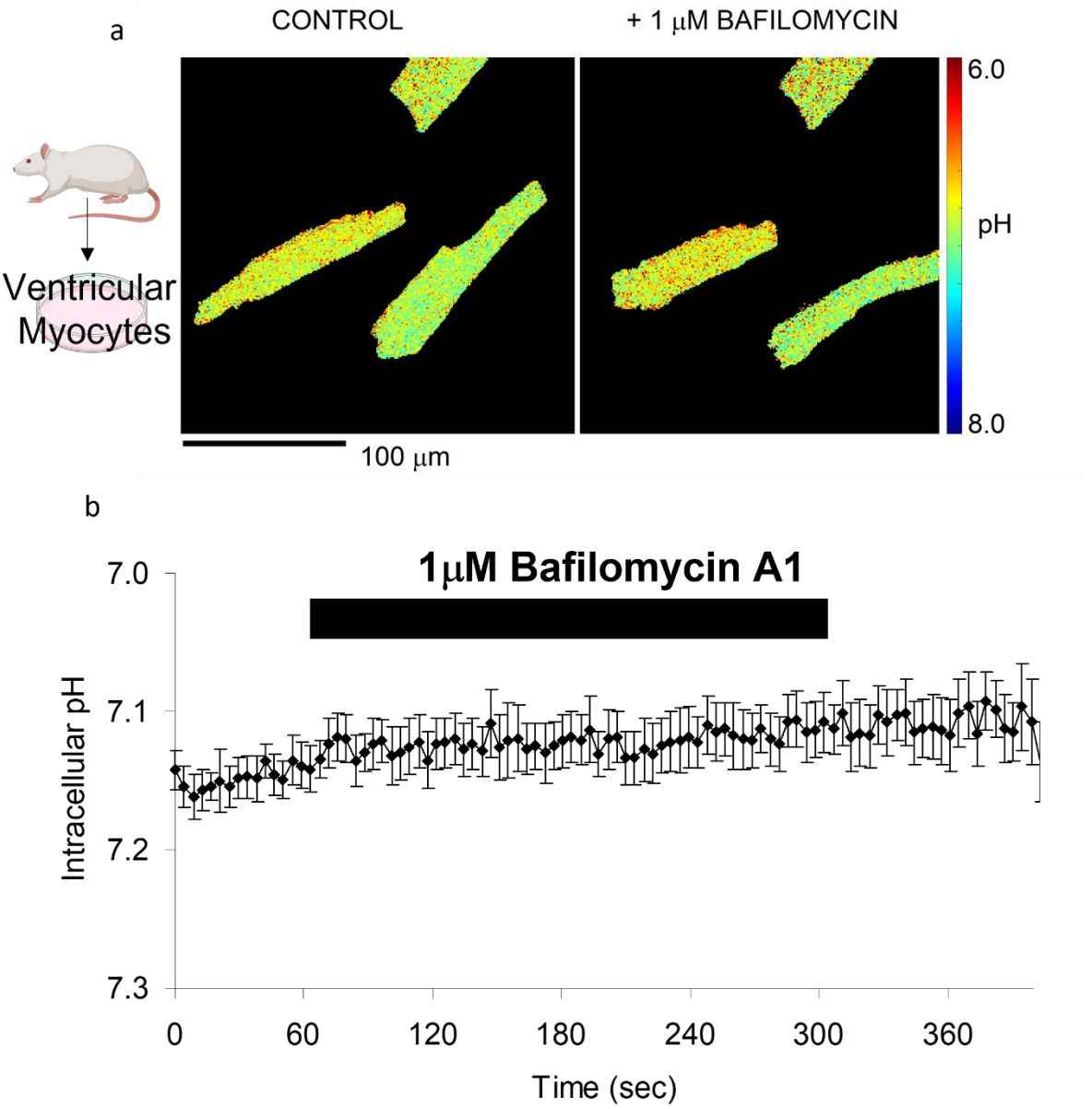

Supplementary Figure 6:

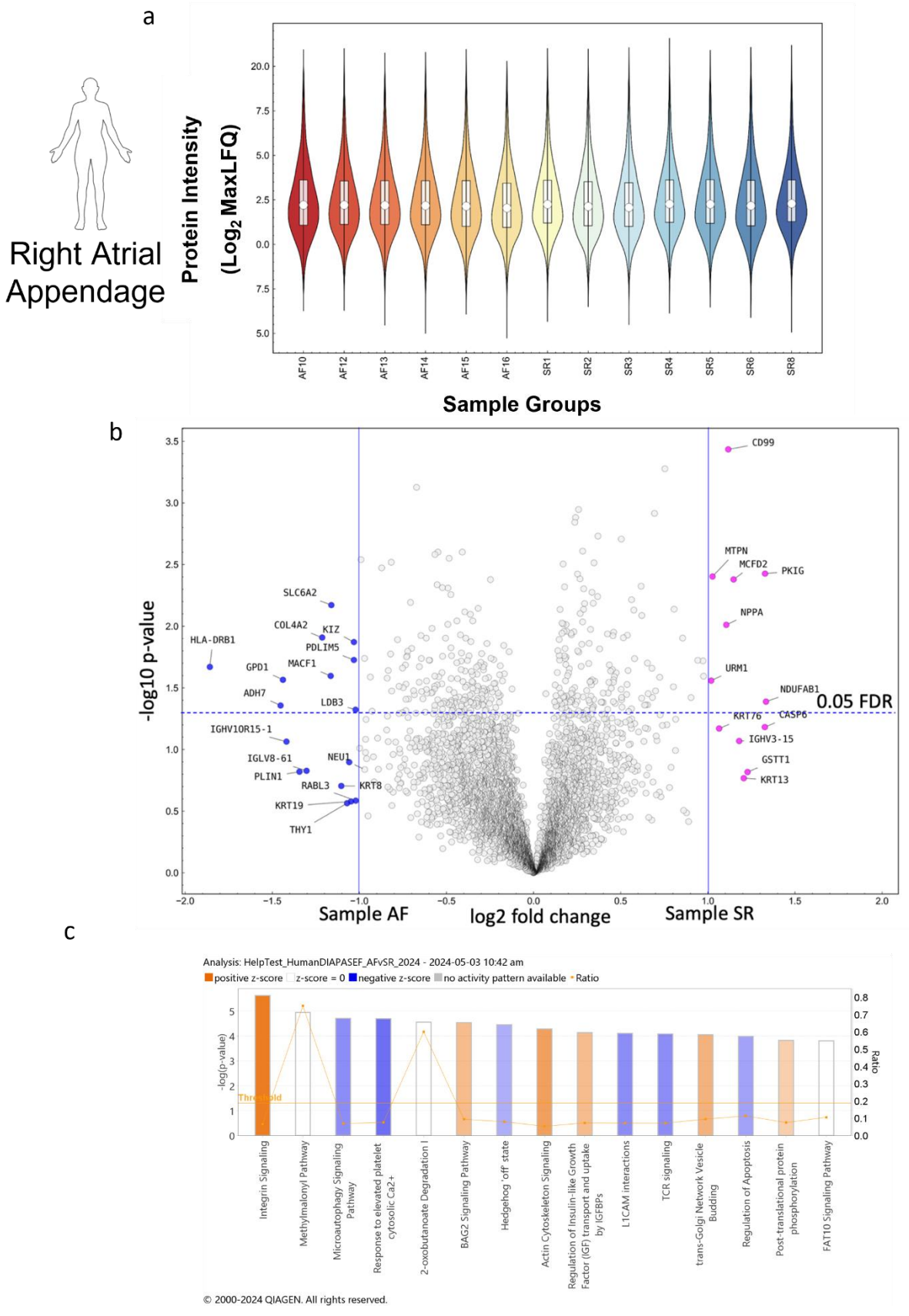

Supplementary Figure 7:

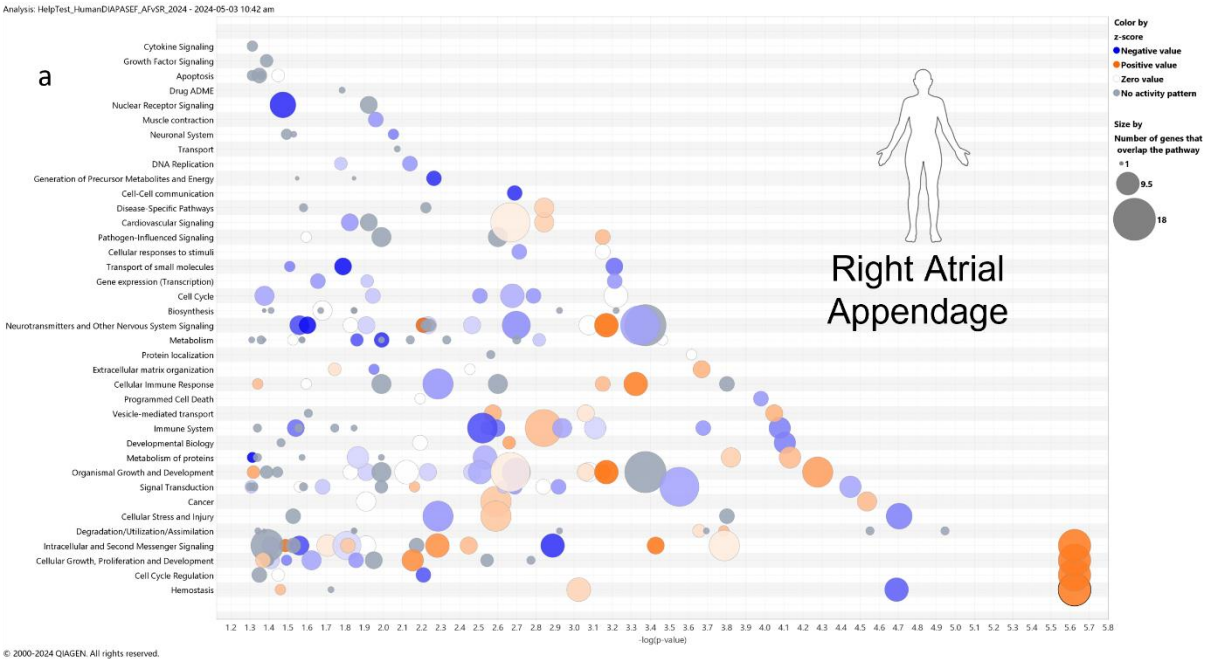

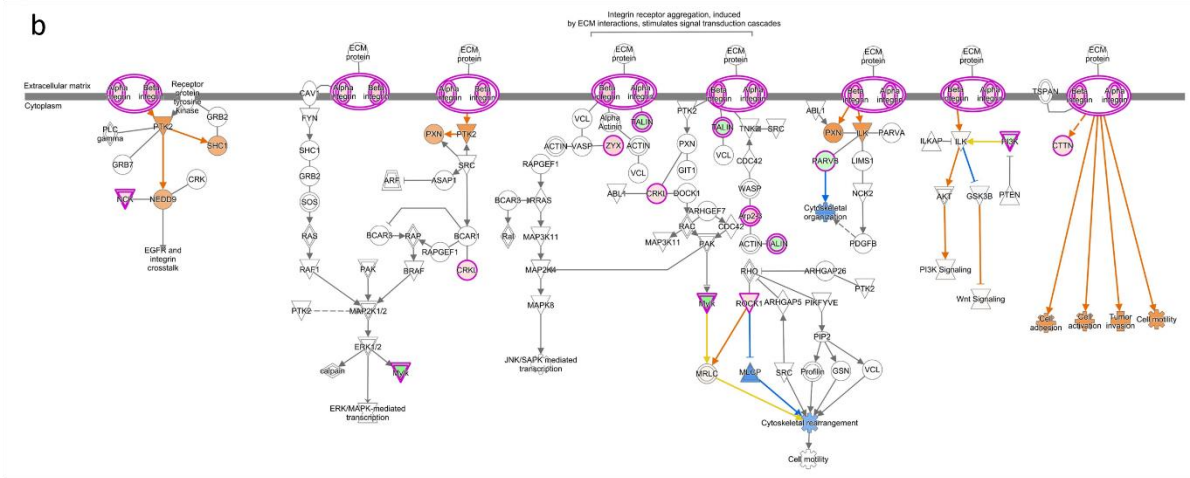

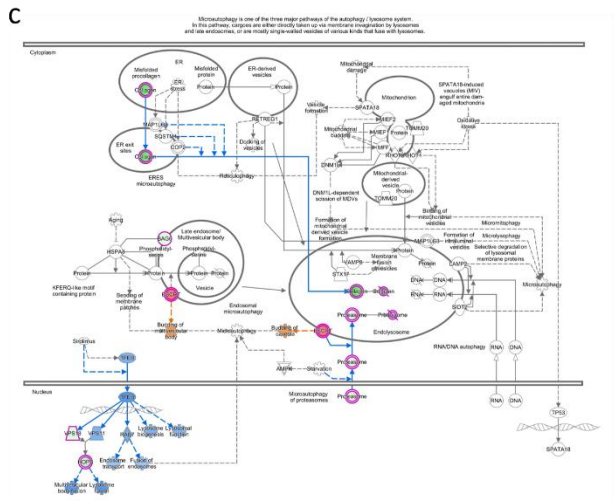

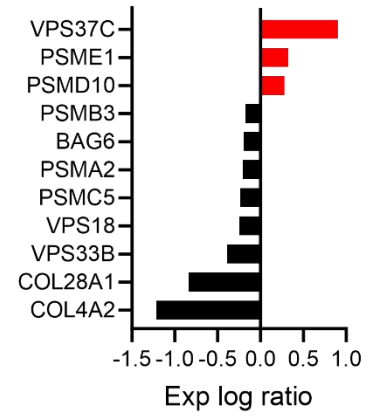

Supplementary Figure 8:

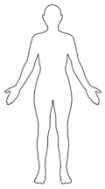

Right Atrial Appendage

a

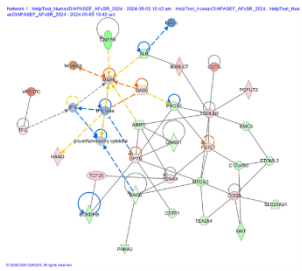

b

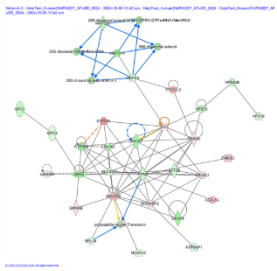

c

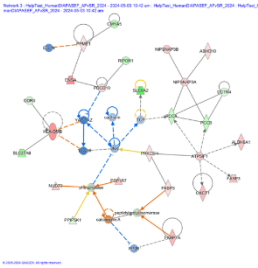

d

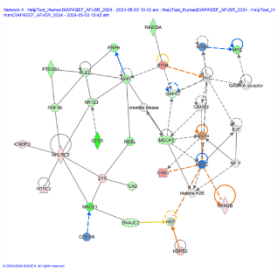

e

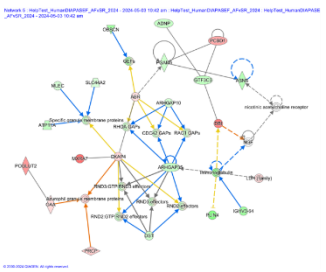

f

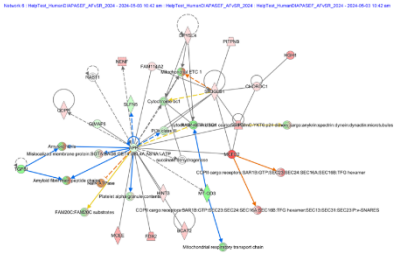

g

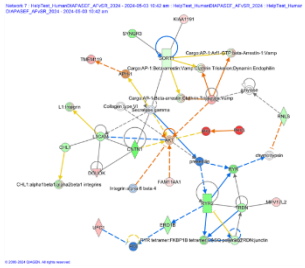

h

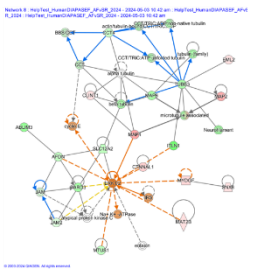

i

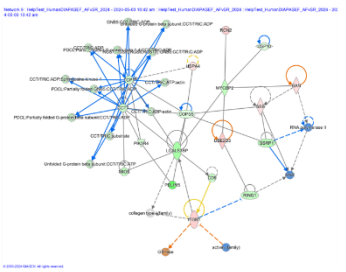

j

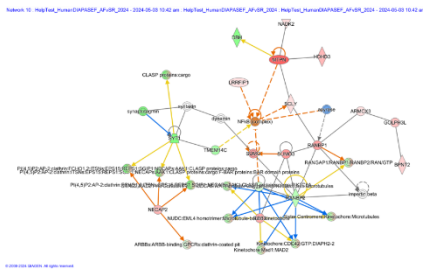

Supplementary Figure 9:

a

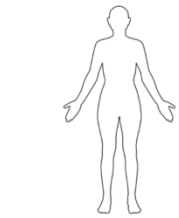

Right Atrial Appendage

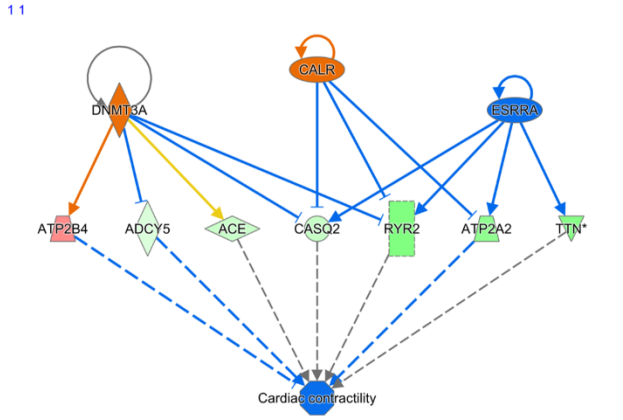

b

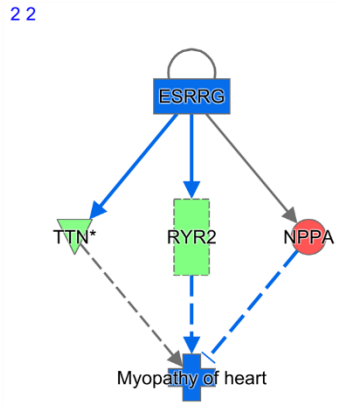

c

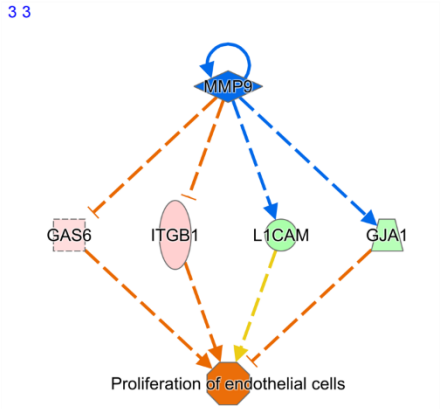

Supplementary Figure 10:

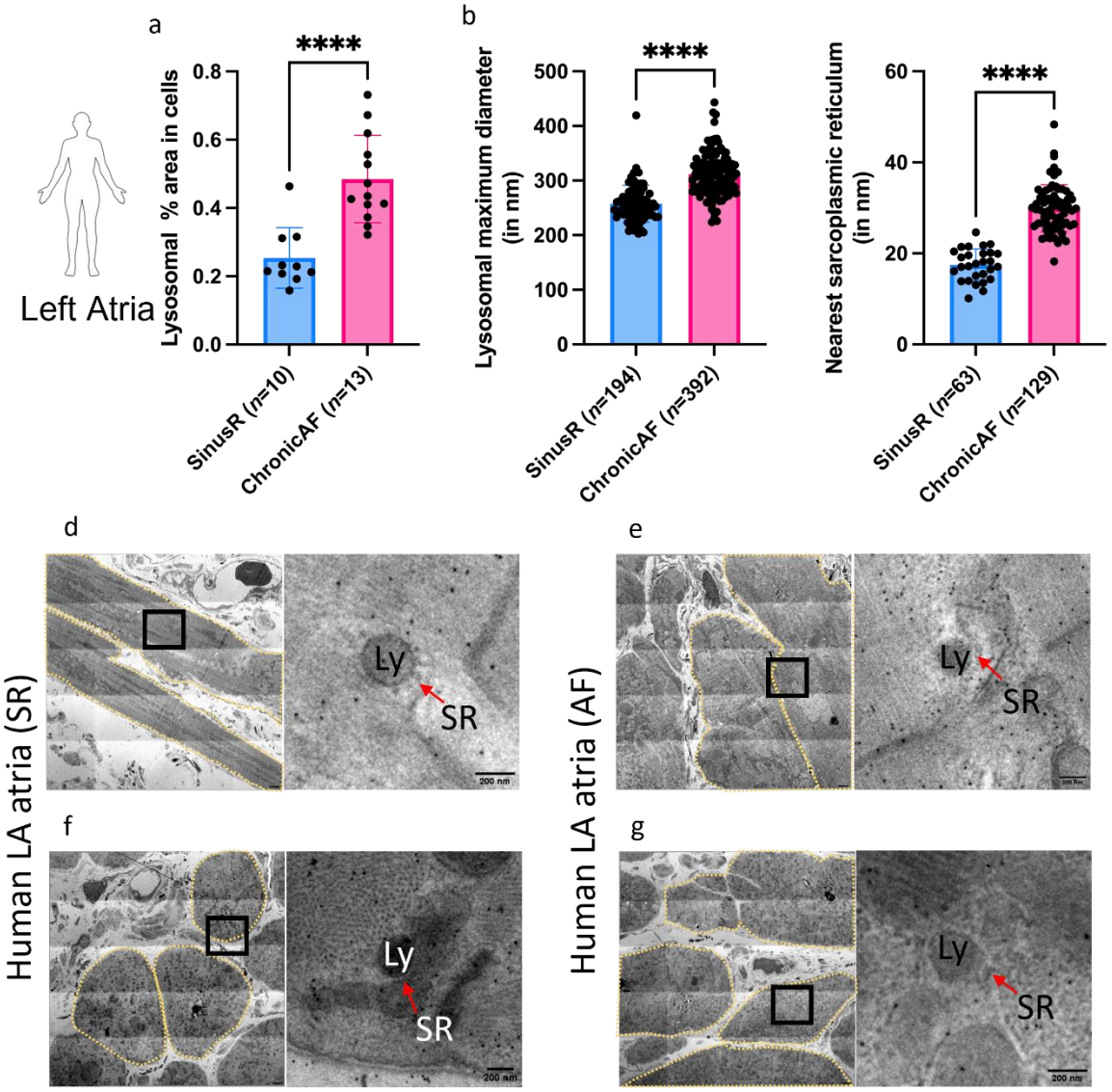

Supplementary Figure 11:

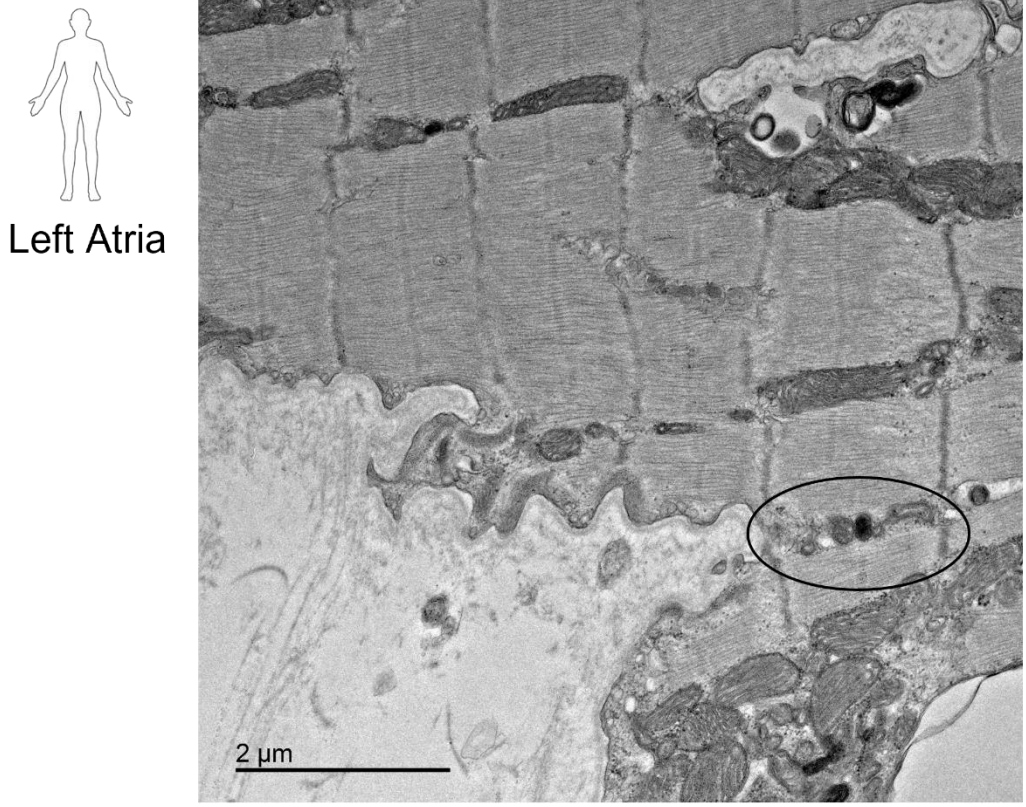

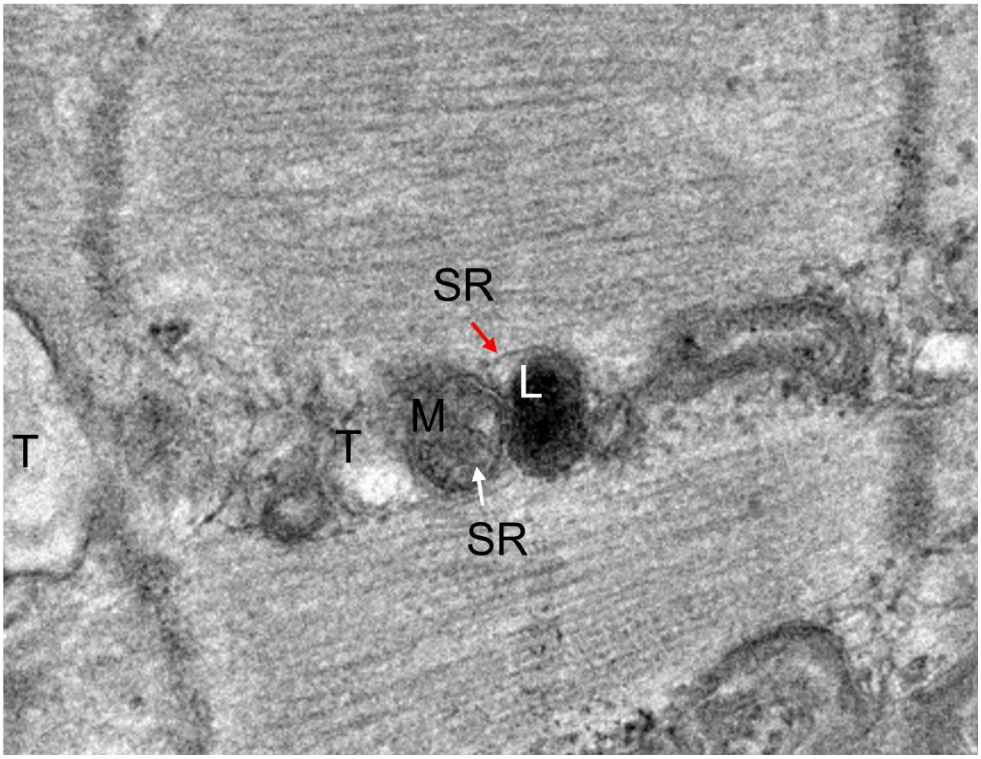

References

1. Wang, Y., et al., *Intracellular β(1)-Adrenergic Receptors and Organic Cation Transporter 3 Mediate Phospholamban Phosphorylation to Enhance Cardiac Contractility.* Circ Res, 2021. **128**(2): p. 246-261.
2. Lee, H.C., *Physiological functions of cyclic ADP-ribose and NAADP as calcium messengers.* Annu Rev Pharmacol Toxicol, 2001. **41**: p. 317-45.
3. Calcraft, P.J., et al., *NAADP mobilizes calcium from acidic organelles through two-pore channels.* Nature, 2009. **459**(7246): p. 596-600.
4. Ruas, M., et al., *Expression of Ca^{2+}-permeable two-pore channels rescues NAADP signalling in TPC-deficient cells.* Embo j, 2015. **34**(13): p. 1743-58.
5. Galione, A., *A primer of NAADP-mediated Ca(2+) signalling: From sea urchin eggs to mammalian cells.* Cell Calcium, 2015. **58**(1): p. 27-47.
6. Macgregor, A., et al., *NAADP controls cross-talk between distinct Ca2+ stores in the heart.* J Biol Chem, 2007. **282**(20): p. 15302-11.
7. Lewis, A.M., et al., *β-Adrenergic receptor signaling increases NAADP and cADPR levels in the heart.* Biochem Biophys Res Commun, 2012. **427**(2): p. 326-9.
8. Gul, R., et al., *Nicotinic Acid Adenine Dinucleotide Phosphate (NAADP) and Cyclic ADP-Ribose (cADPR) Mediate Ca2+ Signaling in Cardiac Hypertrophy Induced by β-Adrenergic Stimulation.* PLoS One, 2016. **11**(3): p. e0149125.
9. Collins, T.P., et al., *NAADP influences excitation-contraction coupling by releasing calcium from lysosomes in atrial myocytes.* Cell Calcium, 2011. **50**(5): p. 449-458.
10. Capel, R.A., et al., *Two-pore Channels (TPC2s) and Nicotinic Acid Adenine Dinucleotide Phosphate (NAADP) at Lysosomal-Sarcoplasmic Reticular Junctions Contribute to Acute and Chronic β-Adrenoceptor Signaling in the Heart.* J Biol Chem, 2015. **290**(50): p. 30087-98.
11. Lakatta, E.G., V.A. Maltsev, and T.M. Vinogradova, *A coupled SYSTEM of intracellular Ca2+ clocks and surface membrane voltage clocks controls the timekeeping mechanism of the heart's pacemaker.* Circ Res, 2010. **106**(4): p. 659-73.
12. Rigg, L., et al., *Modulation of the hyperpolarization-activated current (I(f)) by calcium and calmodulin in the guinea-pig sino-atrial node.* Cardiovasc Res, 2003. **57**(2): p. 497-504.
13. Maltsev, V.A. and E.G. Lakatta, *Synergism of coupled subsarcolemmal Ca2+ clocks and sarcolemmal voltage clocks confers robust and flexible pacemaker function in a novel pacemaker cell model.* Am J Physiol Heart Circ Physiol, 2009. **296**(3): p. H594-615.
14. Rigg, L., et al., *Localisation and functional significance of ryanodine receptors during beta-adrenoceptor stimulation in the guinea-pig sino-atrial node.* Cardiovasc Res, 2000. **48**(2): p. 254-64.
15. Capel, R.A. and D.A. Terrar, *Cytosolic calcium ions exert a major influence on the firing rate and maintenance of pacemaker activity in guinea-pig sinus node.* Front Physiol, 2015. **6**: p. 23.
16. Mattick, P., et al., *Ca2+-stimulated adenylyl cyclase isoform AC1 is preferentially expressed in guinea-pig sino-atrial node cells and modulates the I(f) pacemaker current.* J Physiol, 2007. **582**(Pt 3): p. 1195-203.
17. Younes, A., et al., *Ca(2+) -stimulated basal adenylyl cyclase activity localization in membrane lipid microdomains of cardiac sinoatrial nodal pacemaker cells.* J Biol Chem, 2008. **283**(21): p. 14461-8.
18. Wu, Y. and M.E. Anderson, *CaMKII in sinoatrial node physiology and dysfunction.* Front Pharmacol, 2014. **5**: p. 48.

19. Ayagama, T., et al., *A modified density gradient proteomic-based method to analyze endolysosomal proteins in cardiac tissue*. iScience, 2021. **24**(9): p. 102949.

20. Omatsu-Kanbe, M., T. Yamamoto, and H. Matsuura, *Autophagy is constitutively active in normal mouse sino-atrial nodal cells.* Acta Histochem Cytochem, 2011. **44**(5): p. 223-31.

21. Workman, A.J., *Cardiac adrenergic control and atrial fibrillation.* Naunyn Schmiedebergs Arch Pharmacol, 2010. **381**(3): p. 235-49.

22. Chi, C., A.S. Riching, and K. Song, *Lysosomal Abnormalities in Cardiovascular Disease.* Int J Mol Sci, 2020. **21**(3).

23. Mary-Rabine, L., et al., *The relationship of human atrial cellular electrophysiology to clinical function and ultrastructure.* Circ Res, 1983. **52**(2): p. 188-99.

24. Aston, D., et al., *High resolution structural evidence suggests the Sarcoplasmic Reticulum forms microdomains with Acidic Stores (lysosomes) in the heart.* Sci Rep, 2017. **7**: p. 40620.

25. Collins, T.P., et al., *NAADP influences excitation-contraction coupling by releasing calcium from lysosomes in atrial myocytes.* Cell Calcium, 2011. **50**(5): p. 449-58.

26. Südhof, T.C., et al., *Structure of a novel InsP3 receptor.* Embo j, 1991. **10**(11): p. 3199-206.

27. Lin, W.K., et al., *Synthesis of the Ca(2+)-mobilizing messengers NAADP and cADPR by intracellular CD38 enzyme in the mouse heart: Role in β-adrenoceptor signaling.* J Biol Chem, 2017. **292**(32): p. 13243-13257.

28. Mu-u-min, R.B.A., *Role of Calcium Mobilising Messengers in Cardiac Arrhythmias*. 2019: University of Oxford.

29. Christensen, K.A., J.T. Myers, and J.A. Swanson, *pH-dependent regulation of lysosomal calcium in macrophages.* J Cell Sci, 2002. **115**(Pt 3): p. 599-607.

30. Koschinski, A. and M. Zaccolo, *Activation of PKA in cell requires higher concentration of cAMP than in vitro: implications for compartmentalization of cAMP signalling.* Sci Rep, 2017. **7**(1): p. 14090.

31. Frenzel, H., et al., *Regression of cardiac hypertrophy: Morphometric and biochemical studies in rat heart after swimming training.* Journal of Molecular and Cellular Cardiology, 1988. **20**(8): p. 737-751.

32. Terrin, A., et al., *PGE(1) stimulation of HEK293 cells generates multiple contiguous domains with different [cAMP]: role of compartmentalized phosphodiesterases.* J Cell Biol, 2006. **175**(3): p. 441-51.

33. Klarenbeek, J., et al., *Fourth-generation epac-based FRET sensors for cAMP feature exceptional brightness, photostability and dynamic range: characterization of dedicated sensors for FLIM, for ratiometry and with high affinity.* PLoS One, 2015. **10**(4): p. e0122513.

34. Gerndt, S., et al., *Agonist-mediated switching of ion selectivity in TPC2 differentially promotes lysosomal function.* Elife, 2020. **9**.

35. Penny, C.J., et al., *Coupling acidic organelles with the ER through Ca^{2+} microdomains at membrane contact sites.* Cell Calcium, 2015. **58**(4): p. 387-96.

36. Ayagama, T., et al., *Compartmentalization proteomics revealed endolysosomal protein network changes in a goat model of atrial fibrillation.* iScience, 2024. **27**(6): p. 109609.

37. Wandinger-Ness, A. and M. Zerial, *Rab proteins and the compartmentalization of the endosomal system.* Cold Spring Harb Perspect Biol, 2014. **6**(11): p. a022616.

38. Quintyne, N.J., et al., *Dynactin is required for microtubule anchoring at centrosomes.* J Cell Biol, 1999. **147**(2): p. 321-34.

39. Yuan, Y., et al., *Two-pore channel-2 and inositol trisphosphate receptors coordinate Ca(2+) signals between lysosomes and the endoplasmic reticulum.* Cell Rep, 2024. **43**(1): p. 113628.

40. Mizunami, M., et al., *Roles of calcium/calmodulin-dependent kinase II in long-term memory formation in crickets.* PLoS One, 2014. **9**(9): p. e107442.

41. Anand, A., et al., *Cell Death Induced by Cationic Amphiphilic Drugs Depends on Lysosomal Ca(2+) Release and Cyclic AMP.* Mol Cancer Ther, 2019. **18**(9): p. 1602-1614.

42. Tang, W.J., J. Krupinski, and A.G. Gilman, *Expression and characterization of calmodulin-activated (type I) adenylylcyclase.* J Biol Chem, 1991. **266**(13): p. 8595-603.

43. Wu, Z., S.T. Wong, and D.R. Storms, *Modification of the calcium and calmodulin sensitivity of the type I adenylyl cyclase by mutagenesis of its calmodulin binding domain.* J Biol Chem, 1993. **268**(32): p. 23766-8.

44. Blitzer, R.D., et al., *Gating of CaMKII by cAMP-regulated protein phosphatase activity during LTP.* Science, 1998. **280**(5371): p. 1940-2.

45. Yagishita, S., et al., *A critical time window for dopamine actions on the structural plasticity of dendritic spines.* Science, 2014. **345**(6204): p. 1616-20.

46. Wayman, G.A., et al., *Synergistic activation of the type I adenylyl cyclase by Ca2+ and Gs-coupled receptors in vivo.* J Biol Chem, 1994. **269**(41): p. 25400-5.

47. Mark, G.E. and F.F. Strasser, *Pacemaker activity and mitosis in cultures of newborn rat heart ventricle cells.* Exp Cell Res, 1966. **44**(2): p. 217-33.

48. Ausma, J., et al., *Structural changes of atrial myocardium due to sustained atrial fibrillation in the goat.* Circulation, 1997. **96**(9): p. 3157-63.

49. Davidson, S.M., et al., *Inhibition of NAADP signalling on reperfusion protects the heart by preventing lethal calcium oscillations via two-pore channel 1 and opening of the mitochondrial permeability transition pore.* Cardiovasc Res, 2015. **108**(3): p. 357-66.

50. Verheule, S., et al., *Loss of continuity in the thin epicardial layer because of endomysial fibrosis increases the complexity of atrial fibrillatory conduction.* Circ Arrhythm Electrophysiol, 2013. **6**(1): p. 202-11.

51. Sygitowicz, G., A. Maciejak-Jastrzębska, and D. Sitkiewicz, *A Review of the Molecular Mechanisms Underlying Cardiac Fibrosis and Atrial Fibrillation.* J Clin Med, 2021. **10**(19).

52. Lenski, M., et al., *Cardiac metabolism during atrial fibrillation is characterized by increased lipid accumulation and glycogen synthesis.* European Heart Journal, 2013. **34**(suppl_1).

53. Sun, J., et al., *Decreased propionyl-CoA metabolism facilitates metabolic reprogramming and promotes hepatocellular carcinoma.* Journal of Hepatology, 2023. **78**(3): p. 627-642.

54. Brundel, B.J., et al., *Gene expression of proteins influencing the calcium homeostasis in patients with persistent and paroxysmal atrial fibrillation.* Cardiovasc Res, 1999. **42**(2): p. 443-54.

55. Wakili, R., et al., *Multiple potential molecular contributors to atrial hypocontractility caused by atrial tachycardia remodeling in dogs.* Circ Arrhythm Electrophysiol, 2010. **3**(5): p. 530-41.

56. Ohkusa, T., et al., *Alterations in cardiac sarcoplasmic reticulum Ca2+ regulatory proteins in the atrial tissue of patients with chronic atrial fibrillation.* J Am Coll Cardiol, 1999. **34**(1): p. 255-63.

57. Neef, S., et al., *CaMKII-dependent diastolic SR Ca2+ leak and elevated diastolic Ca2+ levels in right atrial myocardium of patients with atrial fibrillation.* Circ Res, 2010. **106**(6): p. 1134-44.

58. Zhao, Z.H., et al., *Inositol-1,4,5-trisphosphate and ryanodine-dependent Ca2+ signaling in a chronic dog model of atrial fibrillation.* Cardiology, 2007. **107**(4): p. 269-76.

59. Chelu, M.G. and X.H. Wehrens, *Sarcoplasmic reticulum calcium leak and cardiac arrhythmias.* Biochem Soc Trans, 2007. **35**(Pt 5): p. 952-6.

60. Chopra, N., et al., *Ablation of triadin causes loss of cardiac Ca2+ release units, impaired excitation-contraction coupling, and cardiac arrhythmias.* Proc Natl Acad Sci U S A, 2009. **106**(18): p. 7636-41.

61. Yuan, Q., et al., *Sarcoplasmic reticulum calcium overloading in junctin deficiency enhances cardiac contractility but increases ventricular automaticity.* Circulation, 2007. **115**(3): p. 300-9.

62. de Zélicourt, A., et al., *Two-pore channels (TPCs) acts as a hub for excitation-contraction coupling, metabolism and cardiac hypertrophy signalling.* Cell Calcium, 2024. **117**: p. 102839.

63. Jia, W., et al., *Autophagy regulates endoplasmic reticulum homeostasis and calcium mobilization in T lymphocytes.* J Immunol, 2011. **186**(3): p. 1564-74.

64. Capel, R.A., et al., *IP(3)-mediated Ca(2+) release regulates atrial Ca(2+) transients and pacemaker function by stimulation of adenylyl cyclases.* Am J Physiol Heart Circ Physiol, 2021. **320**(1): p. H95-h107.

65. Burton, R.A., et al., *Optical control of excitation waves in cardiac tissue.* Nat Photonics, 2015. **9**(12): p. 813-816.

66. Sigalas, C., et al., *Combining tissue engineering and optical imaging approaches to explore interactions along the neuro-cardiac axis.* R Soc Open Sci, 2020. **7**(6): p. 200265.

67. Winbo, A., et al., *Functional coculture of sympathetic neurons and cardiomyocytes derived from human-induced pluripotent stem cells.* Am J Physiol Heart Circ Physiol, 2020. **319**(5): p. H927-h937.

68. Sharma, A., et al., *Derivation of highly purified cardiomyocytes from human induced pluripotent stem cells using small molecule-modulated differentiation and subsequent glucose starvation.* J Vis Exp, 2015(97).

69. Calamaio, S., et al., *Human iPSC-Derived 3D Hepatic Organoids in a Miniaturized Dynamic Culture System.* Biomedicines, 2023. **11**(8).

70. Benzoni, P., et al., *Human iPSC modelling of a familial form of atrial fibrillation reveals a gain of function of If and ICaL in patient-derived cardiomyocytes.* Cardiovasc Res, 2020. **116**(6): p. 1147-1160.

71. Devalla, H.D., et al., *Atrial-like cardiomyocytes from human pluripotent stem cells are a robust preclinical model for assessing atrial-selective pharmacology.* EMBO Mol Med, 2015. **7**(4): p. 394-410.

72. Moretti, A., et al., *Patient-specific induced pluripotent stem-cell models for long-QT syndrome.* N Engl J Med, 2010. **363**(15): p. 1397-409.

73. Surdo, N.C., et al., *FRET biosensor uncovers cAMP nano-domains at beta-adrenergic targets that dictate precise tuning of cardiac contractility.* Nature Communications, 2017. **8**.

74. Wang, J., et al., *Implementation of a 4Pi-SMS super-resolution microscope.* Nat Protoc, 2021. **16**(2): p. 677-727.

75. van Hunnik, A., et al., *Stationary Atrial Fibrillation Properties in the Goat Do Not Entail Stable or Recurrent Conduction Patterns.* Front Physiol, 2018. **9**: p. 947.

76. Fameli, N., et al., *Cytoplasmic nanojunctions between lysosomes and sarcoplasmic reticulum are required for specific calcium signaling.* F1000Res, 2014. **3**: p. 93.

77. MacDonald, E.A., et al., *Sinoatrial Node Structure, Mechanics, Electrophysiology and the Chronotropic Response to Stretch in Rabbit and Mouse.* Front Physiol, 2020. **11**: p. 809.

78. Rog-Zielinska, E.A., et al., *Species differences in the morphology of transverse tubule openings in cardiomyocytes.* Europace, 2018. **20**(suppl_3): p. iii120-iii124.

79. Swietach, P., et al., *Experimental Generation and Computational Modeling of Intracellular pH Gradients in Cardiac Myocytes.* Biophysical Journal, 2005. **88**(4): p. 3018-3037.

80. Sandow, J.J., et al., *Simplified high-throughput methods for deep proteome analysis on the timsTOF Pro.* bioRxiv, 2021: p. 657908.

81. Nolte, H., et al., *Instant Clue: A Software Suite for Interactive Data Visualization and Analysis.* Sci Rep, 2018. **8**(1): p. 12648.

82. Chandler, N.J., et al., *Molecular architecture of the human sinus node: insights into the function of the cardiac pacemaker.* Circulation, 2009. **119**(12): p. 1562-75.

83. Foskett, J.K., et al., *Inositol trisphosphate receptor Ca2+ release channels.* Physiol Rev, 2007. **87**(2): p. 593-658.

84. Lezoualc'h, F., et al., *Small GTP-binding proteins and their regulators in cardiac hypertrophy.* J Mol Cell Cardiol, 2008. **44**(4): p. 623-32.

85. Cox, J., et al., *Accurate proteome-wide label-free quantification by delayed normalization and maximal peptide ratio extraction, termed MaxLFQ.* Mol Cell Proteomics, 2014. **13**(9): p. 2513-26.